A Second Order Fully-discrete Linear Energy Stable Scheme for a Binary Compressible Viscous Fluid Model

Xueping Zhao*and Qi Wang†

November 29, 2018

Abstract

We present a linear, second order fully discrete numerical scheme on a staggered grid for a thermodynamically consistent hydrodynamic phase field model of binary compressible fluid flow mixtures derived from the generalized Onsager Principle. The hydrodynamic model not only possesses the variational structure, but also warrants the mass, linear momentum conservation as well as energy dissipation. We first reformulate the model in an equivalent form using the energy quadratization method and then discretize the reformulated model to obtain a semi-discrete partial differential equation system using the Crank-Nicolson method in time. The numerical scheme so derived preserves the mass conservation and energy dissipation law at the semi-discrete level. Then, we discretize the semi-discrete PDE system on a staggered grid in space to arrive at a fully discrete scheme using the 2nd order finite difference method, which respects a discrete energy dissipation law. We prove the unique solvability of the linear system resulting from the fully discrete scheme. Mesh refinements and two numerical examples on phase separation due to the spinodal decomposition in two polymeric fluids and interface evolution in the gas-liquid mixture are presented to show the convergence property and the usefulness of the new scheme in applications.

1 Introduction

Material systems comprising of multi-components, some of which are compressible while others are incompressible, are ubiquitous in nature and industrial applications. For example, in growing tissues, cell proliferation makes the material volume changes so that it can not be described as incompressible [20]. Another example of the mixture of compressible fluids is the binary fluid flows of non-hydrocarbon (e.g. CO_2) and hydrocarbons encountered in the enhanced oil recovery(EOR) process. Since gas (e.g. CO_2) injection offers considerable potential benefits to oil recovery and is attracting the most new market interest since 1972, properties (viscosity, density et al.) of multi-component compressible mixtures of nonhydrocarbon and hydrocarbons have been studied by a number of investigators [11, 26, 35].

---

*Department of Mathematics, University of South Carolina, Columbia, SC 29208, USA

†Department of Mathematics, University of South Carolina, Columbia, SC 29208, USA and Beijing Computational Science Research Center, Beijing 100193, China

Phase field methods have been used successfully to formulate models for fluid mixtures in many applications ranging from life sciences [38, 39, 46, 61] (cell biology [22, 33, 38, 55, 62, 63], biofilms [50–52], cell adhesion and motility [6,28,32–34,38], cell membrane [2,3,16,44,47], tumor growth [46]), to materials science [5,7,13], fluid dynamics [29,30,43], image processing [4,25,59] et al. The most widely studied phase field model for binary fluid mixtures is the one for fluid mixtures of two incompressible fluids of identical densities [1, 21, 27]. While modeling binary fluid mixtures using phase field models, one commonly uses a labeling or a phase variable (a volume fraction or a mass fraction) ϕ to distinguish between distinct material phases. For instance $\phi = 1$ indicates one fluid phase while $\phi = 0$ denotes another fluid phase in the immiscible, binary fluid mixture. For immiscible mixtures, the interfacial region is described by $0 < \phi < 1$. A transport equation for the volume fraction ϕ along with conservation equations of mass and momentum constitute the governing system of equations for the binary incompressible fluid mixture.

In the compressible fluid flow, we use the mass density ρ_i or molar density n_i in place of volume fraction ϕ_i $(i = 1, 2)$, to represent the distribution of each compressible component in the fluid mixture. The material compressibility comes from two sources. One is the material compressibility itself and the other is the mass-generating source. In general, the transport equation for the mass density of each component is given by

$$\frac{\partial \rho_i}{\partial t} + \nabla \cdot (\rho_i \mathbf{v_i}) = j_i, \qquad i = 1, \cdots, N, \tag{1.1}$$

or

$$\frac{\partial n_i}{\partial t} + \nabla \cdot (n_i \mathbf{v_i}) = j_i, \qquad i = 1, \cdots, N, \tag{1.2}$$

where $\mathbf{v}_i$ is the velocity of the ith component, j_i is the mass source or molar source of the ith component. The transport equations for the mass or molar densities along with the conservation laws of mass and momentum constitute the governing equations of the hydrodynamic phase field models of the compressible fluid mixtures.

Distinguishing properties of the compressible hydrodynamic phase field models include that the density of each compressible material component is a variable, the mass average velocity of the fluid flow is most likely not solenoidal, and the pressure is determined by the equation of state or the free energy of the mixture system (at least in the isothermal case). In [30], Truskinovsky and Lowengrub derived the Navier−Stokes−Cahn−Hilliard (NSCH) system for a binary mixture of two incompressible fluid flows with unmatched densities in the fluid components, in which the mass concentration of one fluid component in the binary fluid flow is used as the phase variable. They termed the hydrodynamic phase field model quasi-incompressible. In [23, 24], Sun et al. propose a general diffuse interface model with a given equation of state (e.g. Peng-Robinson equation of state) to describe the multi-component fluid flow based on the principles of the NVT-based framework. In [58], we systematically derived a thermodynamically consistent hydrodynamic phase field model for multi-component compressible fluid mixtures through a variational approach coupled with the generalized Onsager Principle [49] and discussed various means to arrive at the quasi-incompressible limit and the fully incompressible limit. In this paper, we develop an unconditionally energy stable numerical algorithm to solve the thermodynamically consistent, hydrodynamic phase field model.

The hydrodynamic phase field model is nonlinear, exemplified in its free energy, mobility coefficients and in the advection in the transport equations. Higher order approximation, unconditional

2

energy stability as well as computational efficiency are desired properties to attain in developing its numerical approximation. To preserve the energy dissipation property, several time-marching approaches have been developed in the past: convex splitting method [8, 10, 14, 15], stabilization method [41, 60], and energy quadratization (EQ, including SAV) approach [19, 19, 54, 57].The convex splitting method has been used to obtain a series of first order energy stable schemes for various PDE models exhibiting energy dissipation properties. However, the convex-splitting scheme is usually nonlinear and therefore can be expensive to solve from time to time. On the other hand, even though it is possible to construct a second order convex splitting scheme in some cases, it was usually done on a case by case basis and a general formulation is not yet available. The stabilization method is another method for obtaining energy stable numerical approximations, which is equivalent to a convex splitting method in some cases. By adding a linear, stablizing operator in the order of the truncation error, one can obtain an energy stable algorithm. In general, a second order stabilizing scheme can be derived, it preserves the discrete energy decay but not the dissipation rate. The energy quadratization(EQ), also known as the invariant energy quadratization(IEQ), method was proposed recently [48] and well developed in various gradient flows and hydrodynamic phase field models [19, 54, 57]. By introducing intermediate variables, one can rewrite the nonlinear free energy functional into a quadratic from, from which a linear second order or even higher order numerical scheme can be constructed [17, 53, 56].

Recently, Sun et al. [23, 24] used the convex splitting approach and the scalar auxiliary variable method [42], which is developed based on the EQ strategy, to solve binary compressible hydrodynamic phase field models, respectively. They obtained some first order semi-discrete schemes. In this paper, we develop a linear, second order, fully discrete numerical scheme for the hydrodynamic phase field model for binary fluid mixtures based on the energy quadratization strategy. We will show that this scheme is unconditionally energy stable and the linear system resulting from the second order numerical scheme is uniquely solvable. At each time step, the linear algebraic system is solved within 3 iterations, with a linear pre-conditioner. Two examples on phase separation dynamics in viscous polymeric blends and interface evolution in gas-liquid mixtures are presented to show the usefulness of the new scheme in some practical applications.

The paper is organized as follows. In §2, we briefly recall the derivation of the compressible hydrodynamic phase field model. Its non-dimensionalization is given in §3. In §4, we reformulate the model using the energy quadratization method. The fully discrete numerical scheme, where we use second order finite difference in space and "linearized" Crank-Nicolson method in time, is given in §5 where the unique solvability of the scheme and the property of energy dissipation are proved as well. In §6, we show several numerical experiments that validate the accuracy, stability and efficiency of the numerical scheme. We give concluding remarks in §7.

2 Thermodynamically Consistent Hydrodynamic Phase Field Models for Binary Compressible Viscous Fluid Flows

A general thermodynamically consistent hydrodynamic phase field model for fluid mixture of n viscous fluid components has been derived in [58]. Here, we brief recall the basic ingredients in the binary fluid model and discuss its energy dissipation property. We consider a fluid mixture flow of two compressible viscous fluids with densities ρ_1 and ρ_2, respectively. The mass conservation

3

equation for each fluid component is respectively given by

$$\frac{\partial \rho_i}{\partial t} + \nabla \cdot (\rho_i \mathbf{v}_i) = 0, \quad i = 1, 2, \tag{2.1}$$

where $\mathbf{v}_i$ is the velocity of the ith fluid component, $i = 1, 2$. We define the total mass of the fluid mixture as $\rho = \rho_1 + \rho_2$ and the mass average velocity as $\mathbf{v} = \frac{1}{\rho}(\rho_1 \mathbf{v}_1 + \rho_2 \mathbf{v}_2)$. Then, the mass conservation equation for the total mass density ρ is given by

$$\frac{\partial \rho}{\partial t} + \nabla \cdot (\rho \mathbf{v}) = 0. \tag{2.2}$$

Using the mass average velocity, we rewrite the mass transport equation as follows

$$\frac{\partial \rho_i}{\partial t} + \nabla \cdot (\rho_i \mathbf{v}) = j_i = \nabla \cdot \mathbf{J}_i, \quad i = 1, 2, \tag{2.3}$$

where $\mathbf{J}_i = \rho_i(\mathbf{v} - \mathbf{v}_i)$ is the excessive mass flux of fluid $i = 1, 2$, and $j_1 + j_2 = 0$ according to the total mass conservation law. The linear momentum conservation law of the fluid mixture is given by

$$\frac{\partial(\rho \mathbf{v})}{\partial t} + \nabla \cdot (\rho \mathbf{v} \mathbf{v}) = \nabla \cdot \sigma + \mathbf{b} \tag{2.4}$$

from the momentum conservation for each fluid component, where $\mathbf{b}$ is the body force, σ is the total stress tensor, $\sigma = \sigma^s + \sigma^e$, σ^s is the symmetric viscous stress tensor, and σ^e is the Ericksen stress tensor. Both $\mathbf{J}_i$, i = 1,2 and σ^s would be determined by constitutive relations later.

For the compressible fluid mixture, we assume the free energy of the system is given by

$$F = \int_V f(\rho_1, \rho_2, \nabla \rho_1, \nabla \rho_2) d\mathbf{x}, \tag{2.5}$$

where f is the free energy density function and V is the domain in which the fluid mixture occupies. The total energy of the fluid system is given by the sum of the kinetic energy and the free energy:

$$E_{total} = \int_V [\tfrac{1}{2} \rho ||\mathbf{v}||^2 + f] d\mathbf{x}. \tag{2.6}$$

Considering the conservation laws of mass and linear momentum, we calculate the energy dissipation rate as follows

$$\frac{dE_{total}}{dt} = \int_V [-\sigma^s : \mathbf{D} + (\mathbf{b} + \nabla \cdot \sigma^e + \rho_1 \nabla \mu_1 + \rho_2 \nabla \mu_2) \cdot \mathbf{v} + \mu_1 j_1 + \mu_2 j_2] d\mathbf{x}$$
$$+ \int_{\partial V} [(\sigma^s \cdot \mathbf{v}) \cdot \mathbf{n} - \tfrac{1}{2}(\rho \mathbf{v} ||\mathbf{v}||^2) \cdot \mathbf{n} + (-\mu_1 \rho_1 \mathbf{v} - \mu_2 \rho_2 \mathbf{v} + \frac{\partial f}{\partial(\nabla \rho_1)} \frac{\partial \rho_1}{\partial t} + \frac{\partial f}{\partial(\nabla \rho_2)} \frac{\partial \rho_2}{\partial t}) \cdot \mathbf{n}] dS. \tag{2.7}$$

where $\mathbf{D} = \frac{1}{2}(\nabla \mathbf{v} + \nabla \mathbf{v}^T)$ is the rate of strain tensor, $\mathbf{n}$ is the unit external normal of the domain boundary ∂V, $\mu_1 = \frac{\partial f}{\partial \rho_1} - \nabla \cdot \frac{\partial f}{\partial \nabla \rho_1}$, $\mu_2 = \frac{\partial f}{\partial \rho_2} - \nabla \cdot \frac{\partial f}{\partial \nabla \rho_2}$ are the chemical potentials with respect to ρ_1 and ρ_2, respectively. We identify the Erickson stress by the equation

$$\nabla \cdot \sigma^e = -\rho_1 \nabla \mu_1 - \rho_2 \nabla \mu_2. \tag{2.8}$$

4

The energy dissipation rate reduces to

$$\frac{dE_{total}}{dt} = \int_V [\mathbf{b} \cdot \mathbf{v} - \sigma^s : \mathbf{D} + \mu_1 j_1 + \mu_2 j_2] d\mathbf{x} + \int_{\partial V} [(\sigma^s \cdot \mathbf{v}) \cdot \mathbf{n} - \frac{1}{2}(\rho \mathbf{v} \|\mathbf{v}\|^2) \cdot \mathbf{n}$$
$$+ (-\mu_1 \rho_1 \mathbf{v} - \mu_2 \rho_2 \mathbf{v} + \frac{\partial f}{\partial(\nabla \rho_1)} \frac{\partial \rho_1}{\partial t} + \frac{\partial f}{\partial(\nabla \rho_2)} \frac{\partial \rho_2}{\partial t}) \cdot \mathbf{n}] dS. \tag{2.9}$$

In the bulk integral, we propose the following constitutive relations following the generalized Onsager principle

$$\sigma^s = 2\eta \mathbf{D} + \bar{\eta} tr(\mathbf{D})\mathbf{I},$$
$$j_i = -\sum_{k=1}^{2} \nabla \cdot M_{ik} \cdot \nabla \mu_k, \tag{2.10}$$

where η, $\bar{\eta}$ are the shear and volumetric viscosity respectively, and $\mathcal{M} = (M_{ik})_{2\times2} \geq 0$ is the symmetric mobility matrix. Since $\sum_{i=1}^{2} j_i = 0$ according to the mass conservation law, this imposes a constraint $\mathcal{M} \cdot \mathbf{1} = \mathbf{0}$, where $\mathbf{1}^T = (1,1)$. Examining the surface integral, we notice that if we assume the following conditions

$$\mathbf{v}|_{\partial V} = 0, \qquad \mathbf{n} \cdot \nabla \mu_i|_{\partial V} = 0, \qquad \mathbf{n} \cdot \frac{\partial f}{\partial(\nabla \rho_i)}|_{\partial V} = 0, \quad i = 1, 2. \tag{2.11}$$

on the boundary, the surface integral vanishes in the energy dissipation function. So, at the absence of the body force $\mathbf{b} = \mathbf{0}$, the total energy dissipation rate reduces to

$$\frac{dE_{total}}{dt} = -\int_V [2\eta \mathbf{D} : \mathbf{D} + \bar{\eta} tr(\mathbf{D})^2 + (\nabla \mu_1, \nabla \mu_2) \cdot \mathcal{M} \cdot (\nabla \mu_1, \nabla \mu_2)^T] d\mathbf{x} \leq 0, \tag{2.12}$$

provided $\eta, \bar{\eta} \geq 0, \mathcal{M} \geq 0$.

Remark 2.1. If we choose the boundary conditions as follows

$$\mathbf{v} \cdot \mathbf{n} = 0, \qquad \sigma_s \cdot \mathbf{n} = -\beta(\mathbf{I} - \mathbf{nn}) \cdot \mathbf{v}, \qquad \mathbf{n} \cdot \frac{\partial f}{\partial(\nabla \rho_1)} = -\gamma_1 \frac{\partial \rho_1}{\partial t}, \qquad \mathbf{n} \cdot \frac{\partial f}{\partial(\nabla \rho_2)} = -\gamma_2 \frac{\partial \rho_2}{\partial t}, \tag{2.13}$$

where $\beta, \gamma_1, \gamma_2 \geq 0$, the energy dissipation rate is given by

$$\frac{dE_{total}}{dt} = -\int_V [2\eta \mathbf{D} : \mathbf{D} + \bar{\eta} tr(\mathbf{D})^2 + (\nabla \mu_1, \nabla \mu_2) \cdot \mathcal{M} \cdot (\nabla \mu_1, \nabla \mu_2)^T] d\mathbf{x}$$
$$- \int_{\partial V} [\beta(\mathbf{I} - \mathbf{nn})\|\mathbf{v}\|^2 + \gamma_1(\frac{\partial \rho_1}{\partial t})^2 + \gamma_2(\frac{\partial \rho_2}{\partial t})^2] ds. \tag{2.14}$$

These boundary conditions allow fluid flows slip at the boundary and mass fluxes to move through the boundary, which leads to additional energy dissipation due to energy dissipation at the surface. We will not pursue these boundary conditions in this study, which worthy of a complete study of its own.

We summarize the governing equations of the compressible binary fluid system in the hydrodynamic phase field model as follows:

$$\begin{cases} \frac{\partial \rho_1}{\partial t} + \nabla \cdot (\rho_1 \mathbf{v}) = \nabla \cdot M_{11} \cdot \nabla \mu_1 + \nabla \cdot M_{12} \cdot \nabla \mu_2, \\ \frac{\partial \rho_2}{\partial t} + \nabla \cdot (\rho_2 \mathbf{v}) = \nabla \cdot M_{21} \cdot \nabla \mu_1 + \nabla \cdot M_{22} \cdot \nabla \mu_2, \\ \frac{\partial(\rho \mathbf{v})}{\partial t} + \nabla \cdot (\rho \mathbf{vv}) = 2\nabla \cdot (\eta \mathbf{D}) + \nabla(\bar{\eta} \nabla \cdot \mathbf{v}) - \rho_1 \nabla \mu_1 - \rho_2 \nabla \mu_2, \end{cases} \tag{2.15}$$

5

where $\sum_{i,k=1}^{2} \nabla \cdot M_{ik} \cdot \nabla \mu_k = 0$. One particular mobility matrix satisfying the constraint is consisted of the entries $M_1 = M_{11} = -M_{12} = -M_{21} = M_{22}$. The governing equations reduce to

$$
\begin{cases}
\frac{\partial \rho_1}{\partial t} + \nabla \cdot (\rho_1 \mathbf{v}) = \nabla \cdot M_1 \cdot \nabla(\mu_1 - \mu_2), \\
\frac{\partial \rho_2}{\partial t} + \nabla \cdot (\rho_2 \mathbf{v}) = -\nabla \cdot M_1 \cdot \nabla(\mu_1 - \mu_2), \\
\frac{\partial (\rho \mathbf{v})}{\partial t} + \nabla \cdot (\rho \mathbf{v} \mathbf{v}) = 2\nabla \cdot (\eta \mathbf{D}) + \nabla(\bar{\eta} \nabla \cdot \mathbf{v}) - \rho_1 \nabla \mu_1 - \rho_2 \nabla \mu_2.
\end{cases}
\tag{2.16}
$$

For the viscosity coefficients, we denote η_1, η_2 as the shear viscosities of the fluid component 1 and 2 respectively, and $\bar{\eta}_1, \bar{\eta}_2$ as the volumetric viscosities of the two components. $\eta, \bar{\eta}$ are chosen as the mass average viscosities of the two components:

$$
\eta = \frac{1}{\rho}[\rho_1 \eta_1 + \rho_2 \eta_2], \qquad \bar{\eta} = \frac{1}{\rho}[\rho_1 \bar{\eta}_1 + \rho_2 \bar{\eta}_2].
\tag{2.17}
$$

In this study, we focus on the free energy density function f in the following form

$$
f(\rho_1, \rho_2, \nabla \rho_1, \nabla \rho_2, T) = h(\rho_1, \rho_2, T) + \frac{1}{2}[\kappa_{\rho_1 \rho_1}(\nabla \rho_1)^2 + 2\kappa_{\rho_1 \rho_2}(\nabla \rho_1, \nabla \rho_2) + \kappa_{\rho_2 \rho_2}(\nabla \rho_2)^2].
\tag{2.18}
$$

where $h(\rho_1, \rho_2, T)$ is the homogeneous or the bulk free energy density function, T is the absolute temperature, assumed a constant in this study, and $\kappa_{\rho_i \rho_j}, i, j = 1, 2$ are model parameters measuring the strength of the conformational entropy (which are assumed constant in this study).

Sometimes, we have to use molar densities n_i as the fundamental variables in the model $i = 1, 2$, system (2.16) can be rewritten as follows

$$
\begin{cases}
m_1(\frac{\partial n_1}{\partial t} + \nabla \cdot (n_1 \mathbf{v})) = \nabla \cdot M_1 \cdot \nabla(\frac{1}{m_1}\mu_{n1} - \frac{1}{m_2}\mu_{n2}), \\
m_2(\frac{\partial n_2}{\partial t} + \nabla \cdot (n_2 \mathbf{v})) = -\nabla \cdot M_1 \cdot \nabla(\frac{1}{m_1}\mu_{n1} - \frac{1}{m_2}\mu_{n2}), \\
\frac{\partial (\rho \mathbf{v})}{\partial t} + \nabla \cdot (\rho \mathbf{v} \mathbf{v}) = 2\nabla \cdot (\eta \mathbf{D}) + \nabla(\bar{\eta} \nabla \cdot \mathbf{v}) - n_1 \nabla \mu_{n1} - n_2 \nabla \mu_{n2},
\end{cases}
\tag{2.19}
$$

where $n_i = \frac{\rho_i}{m_i}$, m_i is the molar mass of the ith component and $\mu_{ni} = \frac{\delta f}{\delta n_i} = \frac{\delta f}{\delta \rho_i} m_i$, i = 1, 2. Correspondingly, The shear and volumetric viscosities are given respectively by $\eta = \sum_{i=1}^{2} \frac{n_i m_i}{n_1 m_1 + n_2 m_2} \eta_i$ and $\bar{\eta} = \sum_{i=1}^{2} \frac{n_i m_i}{n_1 m_1 + n_2 m_2} \bar{\eta}_i$.

With molar densities $n_i, i = 1, 2$ as the primitive variables, we rewrite free energy density f as follows

$$
\begin{aligned}
f(n_1 m_1, n_2 m_2, m_1 \nabla n_1, m_2 \nabla n_2, T) &= h(m_1 n_1, m_2 n_2, T) \\
&+ \frac{1}{2}[\kappa_{n_1 n_1}(\nabla n_1)^2 + 2\kappa_{n_1 n_2}(\nabla n_1, \nabla n_2) + \kappa_{n_2 n_2}(\nabla n_2)^2].
\end{aligned}
\tag{2.20}
$$

Where $\kappa_{n_i n_i} = m_i^2 \kappa_{\rho_i \rho_i}$, i = 1, 2 and $\kappa_{n_1 n_2} = m_1 m_2 \kappa_{\rho_1 \rho_2}$.

The free energy density function is specific to the fluid system studied.

- For polymeric binary fluid mixtures while approximated as a viscous fluid, the Flory-Huggins type free energy density function can be used to describe fluid mixing [12, 30]

$$
h(\rho_1, \rho_2, T) = \frac{k_B T}{m} \rho(\frac{1}{N_1} \frac{\rho_1}{\rho} ln \frac{\rho_1}{\rho} + \frac{1}{N_2} \frac{\rho_2}{\rho} ln \frac{\rho_2}{\rho} + \chi \frac{\rho_1 \rho_2}{\rho^2}),
\tag{2.21}
$$

Where k_B is the Boltzmann constant, T is the absolute temperature and m the average mass of a molecule.

- For compressible gas-liquid mixtures, the semi-empirical Peng-Robinson free energy density is often used [23],

$$h(n_1, n_2, \cdots, n_N, n, T) = f^{ideal} + f^{repulsion} + f^{attraction}, \qquad (2.22)$$

where

$$
\begin{aligned}
f^{ideal} &= RT \sum_{i=1} n_i(ln(n_i) - 1), \\
f^{repulsion} &= -nRTln(1 - bn), \\
f^{attraction} &= \frac{a(T)n}{2\sqrt{2}b} ln\left(\frac{1+(1-\sqrt{2})bn}{1+(1+\sqrt{2})bn}\right).
\end{aligned}
\qquad (2.23)
$$

Here $n = \sum_{i=1}^{N} n_i$ is the total molar density. The corresponding chemical potential of the ith component is given by

$$
\begin{aligned}
\mu_{ni} &= \frac{\partial h}{\partial n_i} - \nabla \cdot \frac{\partial h}{\partial \nabla n_i} = RT\left(ln(n_i) + \frac{b_i n}{1-bn} - ln(1 - bn)\right) + \frac{ab_i n}{b((\sqrt{2}-1)bn-1)(1+(1+\sqrt{2})bn)} \\
&+ \frac{1}{2\sqrt{2}}\left(\frac{2\sum_{j=1}^{M} n_j(a_i a_j)^{1/2}(1-k_{ij})}{bn} - \frac{ab_i}{b^2}\right) ln\left(\frac{1+(1-\sqrt{2})bn}{1+(1+\sqrt{2})bn}\right) - \kappa_{n_i n_i} \Delta n_i - \kappa_{n_i n_j} \Delta n_j, \qquad j \neq i,
\end{aligned}
\qquad (2.24)
$$

where $b(n_1, n_2)$ is the volume parameter and $a(n_1, n_2, T)$ is the interaction parameter. This free energy was proposed to improve that of the Van der Waals' to mitigate the deviation away from the ideal gas model.

3   Non-dimensionalization

For system (2.16), using characteristic time t_0, characteristic length l_0, and characteristic density ρ_0, we nondimensionalize the physical variables and parameters as follows

$$
\begin{aligned}
\tilde{t} &= \frac{t}{t_0}, \quad \tilde{x} = \frac{x}{l_0}, \quad \tilde{\rho}_i = \frac{\rho_i}{\rho_0}, \quad i = 1, 2, \quad \tilde{\mathbf{v}} = \frac{\mathbf{v}t_0}{l_0}, \quad \tilde{M}_1 = \frac{M_1}{t_0\rho_0}, \quad \frac{1}{Re_s} = \tilde{\eta} = \frac{t_0}{\rho_0 l_0^2}\eta, \\
\frac{1}{Re_v} &= \tilde{\bar{\eta}} = \frac{t_0}{\rho_0 l_0^2}\bar{\eta}, \quad \tilde{\mu}_i = \frac{t_0^2}{l_0^2}\mu_i, \quad i = 1, 2, \quad \tilde{\kappa}_{\rho_i \rho_j} = \kappa_{\rho_i \rho_j} \frac{\rho_0 t_0^2}{l_0^4}, \quad i, j = 1, 2,
\end{aligned}
\qquad (3.1)
$$

where Re_s, Re_v are the Reynolds numbers. We rewrite the dimensionless governing equations, after dropping the $\tilde{\ }$s for simplicity, as follows

$$
\begin{cases}
\frac{\partial \rho_1}{\partial t} + \nabla \cdot (\rho_1 \mathbf{v}) = \nabla \cdot M_1 \cdot \nabla(\mu_1 - \mu_2), \\
\frac{\partial \rho_2}{\partial t} + \nabla \cdot (\rho_2 \mathbf{v}) = -\nabla \cdot M_1 \cdot \nabla(\mu_1 - \mu_2), \\
\frac{\partial(\rho \mathbf{v})}{\partial t} + \nabla \cdot (\rho \mathbf{v}\mathbf{v}) = 2\nabla \cdot (\frac{1}{Re_s}\mathbf{D}) + \nabla(\frac{1}{Re_v}\nabla \cdot \mathbf{v}) - \rho_1 \nabla\mu_1 - \rho_2 \nabla\mu_2.
\end{cases}
\qquad (3.2)
$$

where

$$\mu_1 = \frac{\partial h}{\partial \rho_1} - \kappa_{\rho_1 \rho_1}\Delta\rho_1 - \kappa_{\rho_1 \rho_2}\Delta\rho_2, \qquad \mu_2 = \frac{\partial h}{\partial \rho_2} - \kappa_{\rho_1 \rho_2}\Delta\rho_1 - \kappa_{\rho_2 \rho_2}\Delta\rho_2. \qquad (3.3)$$

Similarly, for system (2.19) with molar density as fundamental variables, using characteristic molar density n_0 $(mol \cdot m^{-d})$, characteristic mass density $\rho_0 = n_0 m_2 (kg \cdot m^{-d}, d = 3)$ and characteristic temperature T_0 (Kelvin), we nondimensionalize the physical variables and parameters as follows

$$\tilde{t} = \frac{t}{t_0}, \quad \tilde{x} = \frac{x}{l_0}, \quad \tilde{\rho} = \frac{\rho}{\rho_0}, \quad \tilde{n} = \frac{n}{n_0}, \quad \tilde{T} = \frac{T}{T_0}, \quad \frac{1}{Re_s} = \tilde{\eta} = \frac{t_0}{\rho_0 l_0^2}\eta, \quad \tilde{m_1} = \frac{m_1 n_0}{\rho_0}, \quad \tilde{m_2} = \frac{m_2 n_0}{\rho_0},$$

$$\frac{1}{Re_v} = \tilde{\overline{\eta}} = \frac{t_0}{\rho_0 l_0^2}\overline{\eta}, \quad \tilde{\mu}_{ni} = \frac{n_0 t_0^2}{\rho_0 l_0^2}\mu_{ni}, \quad i = 1, 2, \quad \tilde{M_1} = \frac{M_1}{t_0 \rho_0}, \quad \tilde{\kappa_{n_i n_j}} = \kappa_{n_i n_j}\frac{n_0^2 t_0^2}{\rho_0 l_0^4}, \quad i, j = 1, 2. \tag{3.4}$$

Dropping $\tilde{\ }$'s for simplicity, we rewrite the dimensionless governing equations as follows

$$\begin{cases} m_1(\frac{\partial n_1}{\partial t} + \nabla \cdot (n_1 \mathbf{v})) = \nabla \cdot M_1 \cdot \nabla(\frac{1}{m_1}\mu_{n1} - \mu_{n2}), \\ (\frac{\partial n_2}{\partial t} + \nabla \cdot (n_2 \mathbf{v})) = -\nabla \cdot M_1 \cdot \nabla(\frac{1}{m_1}\mu_{n1} - \mu_{n2}), \\ \frac{\partial(\rho \mathbf{v})}{\partial t} + \nabla \cdot (\rho \mathbf{v} \mathbf{v}) = 2\nabla \cdot (\eta \mathbf{D}) + \nabla(\overline{\eta}\nabla \cdot \mathbf{v}) - n_1 \nabla \mu_{n1} - n_2 \nabla \mu_{n2}. \end{cases} \tag{3.5}$$

where we set $\tilde{m_2} = \frac{m_2 n_0}{\rho_0} = 1$, i.e. m_1 is the ratio of the specific masses, a dimensionless model parameter. The dimensionless chemical potentials are given by

$$\mu_{n1} = \frac{\partial h}{\partial n_1} - \kappa_{n_1 n_1}\Delta n_1 - \kappa_{n_1 n_2}\Delta n_2, \qquad \mu_{n2} = \frac{\partial h}{\partial n_2} - \kappa_{n_1 n_2}\Delta n_1 - \kappa_{n_2 n_2}\Delta n_2. \tag{3.6}$$

In the following, we focus on developing an energy stable numerical scheme for system (3.2) on staggered grids. An energy stable numerical scheme for system (3.5) can be obtained analogously. First, we reformulate the equation system using the energy quadratization strategy.

4 Reformulation of the Model using Energy Quadratization

In order to use the Energy Quadratization (EQ) method to design numerical schemes, we need to reformulate the model equations. We first transform the energy of the system into a quadratic form

$$E_{total} = \int_V [\frac{1}{2}\rho \mathbf{v}^T \mathbf{v} + f]d\mathbf{x} = \int_V [\frac{1}{2}\mathbf{u}^T \mathbf{u} + q_1^2 + \frac{1}{2}\mathbf{p}^T \cdot \mathbf{K} \cdot \mathbf{p} - A]d\mathbf{x}. \tag{4.1}$$

where $\mathbf{u} = \sqrt{\rho}\mathbf{v}$, $q_1 = \sqrt{h(\rho_1, \rho_2, T) + A}$ and A is a constant such that $h(\rho_1, \rho_2, T) + A > 0$. We note that we can always find a constant A if the bulk free energy density function is bounded below. In addition, $\mathbf{p} = (\nabla \rho_1, \nabla \rho_2)^T$ and $\mathbf{K}$ is the coefficient matrix of the conformational entropy

$$\mathbf{K} = \begin{pmatrix} \kappa_{\rho_1 \rho_1} & \kappa_{\rho_1 \rho_2} \\ \kappa_{\rho_1 \rho_2} & \kappa_{\rho_2 \rho_2} \end{pmatrix} > 0. \tag{4.2}$$

Using identity

$$\frac{\partial(\sqrt{\rho}\mathbf{u})}{\partial t} = \frac{1}{2\sqrt{\rho}}\frac{\partial \rho}{\partial t}\mathbf{u} + \sqrt{\rho}\frac{\partial \mathbf{u}}{\partial t} = -\frac{1}{2\sqrt{\rho}}\nabla \cdot (\sqrt{\rho}\mathbf{u})\mathbf{u} + \sqrt{\rho}\frac{\partial \mathbf{u}}{\partial t}, \tag{4.3}$$

8

we rewrite the governing equations into

$$
\begin{cases}
\frac{\partial \rho_1}{\partial t} + \nabla \cdot (\frac{\rho_1}{\sqrt{\rho}}\mathbf{u}) = \nabla \cdot M_1 \cdot \nabla(\mu_1 - \mu_2), \\
\frac{\partial \rho_2}{\partial t} + \nabla \cdot (\frac{\rho_2}{\sqrt{\rho}}\mathbf{u}) = -\nabla \cdot M_1 \cdot \nabla(\mu_1 - \mu_2), \\
\frac{\partial \mathbf{u}}{\partial t} + \frac{1}{2}(\frac{1}{\sqrt{\rho}}\nabla \cdot (\mathbf{u}\mathbf{u}) + \mathbf{u}\cdot\nabla\frac{\mathbf{u}}{\sqrt{\rho}}) = \frac{1}{\sqrt{\rho}}\nabla\cdot\sigma, \\
\frac{\partial q_1}{\partial t} = \frac{\partial q_1}{\partial \rho_1}\frac{\partial \rho_1}{\partial t} + \frac{\partial q_1}{\partial \rho_2}\frac{\partial \rho_2}{\partial t},
\end{cases}
\tag{4.4}
$$

where

$$
\begin{aligned}
&\sigma = \sigma^s + \sigma^e, \quad \sigma^s = 2\frac{1}{Re_s}\mathbf{D} + \frac{1}{Re_v}(\nabla\cdot\frac{\mathbf{u}}{\sqrt{\rho}})\mathbf{I}, \\
&\sigma^e = (f - \rho_1\mu_1 - \rho_2\mu_2)\mathbf{I} - \frac{\partial f}{\partial\nabla\rho_1}\nabla\rho_1 - \frac{\partial f}{\partial\nabla\rho_2}\nabla\rho_2, \\
&\nabla\cdot\sigma = \nabla\cdot(\sigma^s + \sigma^e) = 2\nabla\cdot(\frac{1}{Re_s}\mathbf{D}) + \nabla(\frac{1}{Re_v}\nabla\cdot\frac{\mathbf{u}}{\sqrt{\rho}}) - \rho_1\nabla\mu_1 - \rho_2\nabla\mu_2, \\
&\mu_1 = \frac{\delta f}{\delta\rho_1} = \frac{\partial f}{\partial\rho_1} - \nabla\cdot\frac{\partial f}{\partial\nabla\rho_1} = 2q_1\frac{\partial q_1}{\partial\rho_1} - \kappa_{\rho_1\rho_1}\Delta\rho_1 - \kappa_{\rho_1\rho_2}\Delta\rho_2, \\
&\mu_2 = \frac{\delta f}{\delta\rho_2} = \frac{\partial f}{\partial\rho_2} - \nabla\cdot\frac{\partial f}{\partial\nabla\rho_2} = 2q_1\frac{\partial q_1}{\partial\rho_2} - \kappa_{\rho_2\rho_2}\Delta\rho_2 - \kappa_{\rho_1\rho_2}\Delta\rho_1, \\
&\mathbf{D} = \frac{1}{2}(\nabla\frac{\mathbf{u}}{\sqrt{\rho}} + (\nabla\frac{\mathbf{u}}{\sqrt{\rho}})^T), \quad \frac{1}{Re_s} = \frac{\rho_1}{\rho}\frac{1}{Re_{s1}} + \frac{\rho_2}{\rho}\frac{1}{Re_{s2}}, \quad \frac{1}{Re_v} = \frac{\rho_1}{\rho}\frac{1}{Re_{v1}} + \frac{\rho_2}{\rho}\frac{1}{Re_{v2}}.
\end{aligned}
\tag{4.5}
$$

Remark 4.1. We define the inner product of two functions f and g as follows:

$$
(f, g) = \int_V fg d\mathbf{x}.
\tag{4.6}
$$

Theorem 4.1. System (4.4) is dissipative, and the corresponding energy dissipation rate is given by

$$
\frac{\partial E}{\partial t} = -2(\frac{1}{Re_s}, \mathbf{D}:\mathbf{D}) - (\frac{1}{Re_v}\nabla\cdot\frac{\mathbf{u}}{\sqrt{\rho}}, \nabla\cdot\frac{\mathbf{u}}{\sqrt{\rho}}) - (\nabla\mu_1, \nabla\mu_2)\cdot\mathcal{M}\cdot(\nabla\mu_1, \nabla\mu_2)^T \le 0,
\tag{4.7}
$$

where $Re_s, Re_v \ge 0, \mathcal{M} = \begin{pmatrix} M_1 & -M_1 \\ -M_1 & M_1 \end{pmatrix} \ge 0.$

Proof: By the definition of E, we have

$$
\frac{\partial E}{\partial t} = \int_V \left[\mathbf{u}^T\frac{\partial\mathbf{u}}{\partial t} + 2q_1\frac{\partial q_1}{\partial t} + (\nabla\rho_1, \nabla\rho_2)\cdot\mathbf{K}\cdot(\nabla\frac{\partial\rho_1}{\partial t}, \nabla\frac{\partial\rho_2}{\partial t})^T\right]d\mathbf{x}.
\tag{4.8}
$$

Taking the inner product of (4.4-3) with $\mathbf{u}$ and using integration by parts, we obtain

$$
(\mathbf{u}, \frac{\partial\mathbf{u}}{\partial t}) = -2(\frac{1}{Re_s}, \mathbf{D}:\mathbf{D}) - (\frac{1}{Re_v}\nabla\cdot\frac{\mathbf{u}}{\sqrt{\rho}}, \nabla\cdot\frac{\mathbf{u}}{\sqrt{\rho}}) - (\mathbf{u}, \rho_1\frac{1}{\sqrt{\rho}}\nabla\mu_1 + \rho_2\frac{1}{\sqrt{\rho}}\nabla\mu_2).
\tag{4.9}
$$

Taking the inner product of (4.4-4) with $2q_1$, using the identities of μ_i, i= 1,2, and performing integration by parts, we obtain

$$
\begin{aligned}
(2q_1, \frac{\partial q_1}{\partial t}) = &-(\nabla\mu_1, \nabla\mu_2)\cdot\mathcal{M}\cdot(\nabla\mu_1, \nabla\mu_2)^T + (\frac{\rho_1}{\sqrt{\rho}}\mathbf{u}, \nabla\mu_1) + (\frac{\rho_2}{\sqrt{\rho}}\mathbf{u}, \nabla\mu_2) \\
&-(\nabla\rho_1, \nabla\rho_2)\cdot\mathbf{K}\cdot(\nabla\frac{\partial\rho_1}{\partial t}, \nabla\frac{\partial\rho_2}{\partial t})^T.
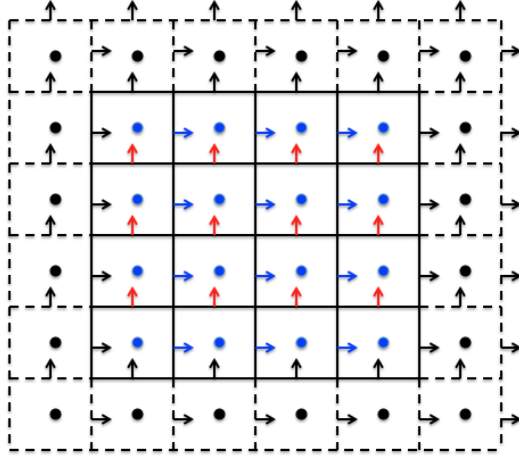\end{aligned}
\tag{4.10}
$$

Figure 5.1: Staggered grid in 2D space.

Combining (4.9) and (4.10), we obtain

$$\frac{\partial E}{\partial t} = -2(\frac{1}{Re_s}, \mathbf{D}:\mathbf{D}) - (\frac{1}{Re_v}\nabla \cdot \frac{\mathbf{u}}{\sqrt{\rho}}, \nabla \cdot \frac{\mathbf{u}}{\sqrt{\rho}}) - (\nabla\mu_1, \nabla\mu_2) \cdot \mathcal{M} \cdot (\nabla\mu_1, \nabla\mu_2)^T \leq 0 \qquad (4.11)$$

provided $\mathcal{M} \geq 0$.

We next design a second order energy stable numerical scheme based on the reformulated governing system of equations.

5 Linear, Second Order Energy Stable Numerical Scheme

5.1 Notations and Useful Lemmas

We first introduce some notations, finite difference operators and useful lemmas. Here, we follow the notations in [9,40,45]. Let $\Omega = [0, L_x] \times [0, L_y]$ be the computational domain with $L_x = h_x \times N_x$, $L_y = h_y \times N_y$, where N_x, N_y are positive integers, and h_x, h_y are spatial step sizes in the x and y direction, respectively. We define three sets for the grid points as follows

$$
\begin{aligned}
E_x &:= \{x_{i+1/2} = i \cdot h \quad | \quad i = 0, 1, \cdots, N_x\}, \\
C_x &:= \{x_i = (i - \tfrac{1}{2}) \cdot h \quad | \quad i = 1, \cdots, N_x\}, \\
C_{\overline{x}} &:= \{x_i = (i - \tfrac{1}{2}) \cdot h \quad | \quad i = 0, 1, \cdots, N_x, N_x + 1\},
\end{aligned}
\qquad (5.1)
$$

where E_x is a uniform partition of $[0, L_x]$ of size N_x in the x-direction and its elements are called edge-centered points. The elements of C_x and $C_{\overline{x}}$ are called cell-centered points. The two points belonging to $C_{\overline{x}} \backslash C_x$ are called ghost points. Analogously, we define E_y as the uniform partition of $[0, L_y]$ of size N_y, called edge-centered points in the y-direction, and $C_y, C_{\overline{y}}$ the cell-centered

points of the interval $[0, L_y]$. In Figure 5.1, we show the staggered grid in 2D space. In this paper, we discretize the variables with the Neumann boundary conditions at the cell-center and the ones with the Dirichlet boundary conditions at the edge-center. We define the corresponding discrete function space on this staggered grid as follows

$$\mathcal{C}_{x \times y} := \{\phi : C_x \times C_y \to \mathcal{R}\}, \quad \mathcal{C}_{\overline{x} \times y} := \{\phi : C_{\overline{x}} \times C_y \to \mathcal{R}\}, \quad \mathcal{C}_{x \times \overline{y}} := \{\phi : C_x \times C_{\overline{y}} \to \mathcal{R}\},$$

$$\mathcal{C}_{\overline{x} \times \overline{y}} := \{\phi : C_{\overline{x}} \times C_{\overline{y}} \to \mathcal{R}\}, \quad \mathcal{E}_{x \times y}^{ew} := \{\phi : E_x \times C_y \to \mathcal{R}\}, \quad \mathcal{E}_{x \times \overline{y}}^{ew} := \{\phi : E_x \times C_{\overline{y}} \to \mathcal{R}\}, \quad (5.2)$$

$$\mathcal{E}_{x \times y}^{ns} := \{\phi : C_x \times E_y \to \mathcal{R}\}, \quad \mathcal{E}_{\overline{x} \times y}^{ns} := \{\phi : C_{\overline{x}} \times E_y \to \mathcal{R}\}, \quad \mathcal{V}_{x \times y} := \{\phi : E_x \times E_y \to \mathcal{R}\}.$$

$\mathcal{C}_{x \times y}, \mathcal{C}_{\overline{x} \times y}, \mathcal{C}_{x \times \overline{y}}$ and $\mathcal{C}_{\overline{x} \times \overline{y}}$ are the sets for discrete cell-centered functions, and $\mathcal{E}_{x \times y}^{ew}, \mathcal{E}_{x \times y}^{ns}$ east-west and north-south edge-centered functions, respectively.

5.1.1 Average and Difference Operators

Assume $u, r \in \mathcal{E}_{x \times y}^{ew} \cup \mathcal{E}_{x \times \overline{y}}^{ew}$, $v, w \in \mathcal{E}_{x \times y}^{ns} \cup \mathcal{E}_{\overline{x} \times y}^{ns}$, $\phi, \psi \in \mathcal{C}_{x \times y} \cup \mathcal{C}_{\overline{x} \times y} \cup \mathcal{C}_{x \times \overline{y}} \cup \mathcal{C}_{\overline{x} \times \overline{y}}$ and $f \in \mathcal{V}_{x \times y}$, we define the east-west-edge-to-center average and difference operator as $a_x, d_x : \mathcal{E}_{x \times \overline{y}}^{ew} \cup \mathcal{V}_{x \times y} \to \mathcal{C}_{x \times \overline{y}} \cup \mathcal{E}_{x \times y}^{ns}$ component-wise as follows

$$a_x u_{i,j} := \tfrac{1}{2}(u_{i+\frac{1}{2},j} + u_{i-\frac{1}{2},j}), \quad d_x u_{i,j} := \tfrac{1}{h_x}(u_{i+\frac{1}{2},j} - u_{i-\frac{1}{2},j}),$$

$$a_x f_{i,j+\frac{1}{2}} := \tfrac{1}{2}(f_{i+\frac{1}{2},j+\frac{1}{2}} + f_{i-\frac{1}{2},j+\frac{1}{2}}), \quad d_x f_{i,j+\frac{1}{2}} := \tfrac{1}{h_x}(f_{i+\frac{1}{2},j+\frac{1}{2}} - f_{i-\frac{1}{2},j+\frac{1}{2}}). \quad (5.3)$$

The north-south-edge-to-center average and difference operators are defined as $a_y, d_y : \mathcal{E}_{\overline{x} \times y}^{ns} \cup \mathcal{V}_{x \times y} \to \mathcal{C}_{\overline{x} \times y} \cup \mathcal{E}_{x \times y}^{ew}$ component-wise as follows

$$a_y v_{i,j} := \tfrac{1}{2}(v_{i,j+\frac{1}{2}} + v_{i,j-\frac{1}{2}}), \quad d_y v_{i,j} := \tfrac{1}{h_y}(v_{i,j+\frac{1}{2}} - v_{i,j-\frac{1}{2}}),$$

$$a_y f_{i+\frac{1}{2},j} := \tfrac{1}{2}(f_{i+\frac{1}{2},j+\frac{1}{2}} + f_{i+\frac{1}{2},j-\frac{1}{2}}), \quad d_y f_{i+\frac{1}{2},j} := \tfrac{1}{h_y}(f_{i+\frac{1}{2},j+\frac{1}{2}} - f_{i+\frac{1}{2},j-\frac{1}{2}}). \quad (5.4)$$

We denote the center-to-east-west-edge average and difference operators as $A_x, D_x : \mathcal{C}_{\overline{x} \times \overline{y}} \cup \mathcal{E}_{\overline{x} \times y}^{ns} \to \mathcal{E}_{x \times \overline{y}}^{ew} \cup \mathcal{V}_{x \times y}$ in component-wise forms:

$$A_x \phi_{i+\frac{1}{2},j} := \tfrac{1}{2}(\phi_{i+1,j} + \phi_{i,j}), \quad D_x \phi_{i+\frac{1}{2},j} := \tfrac{1}{h_x}(\phi_{i+1,j} - \phi_{i,j}),$$

$$A_x v_{i+\frac{1}{2},j+\frac{1}{2}} := \tfrac{1}{2}(v_{i+1,j+\frac{1}{2}} + v_{i,j+\frac{1}{2}}), \quad D_x v_{i+\frac{1}{2},j+\frac{1}{2}} := \tfrac{1}{h_x}(v_{i+1,j+\frac{1}{2}} - v_{i,j+\frac{1}{2}}). \quad (5.5)$$

Analogously, the center-to-north-south-edge average and difference operator are defined as $A_y, D_y : \mathcal{C}_{\overline{x} \times \overline{y}} \cup \mathcal{E}_{x \times \overline{y}}^{ew} \to \mathcal{E}_{\overline{x} \times y}^{ns} \cup \mathcal{V}_{x \times y}$ in component-wise forms:

$$A_y \phi_{i,j+\frac{1}{2}} := \tfrac{1}{2}(\phi_{i,j+1} + \phi_{i,j}), \quad D_y \phi_{i,j+\frac{1}{2}} := \tfrac{1}{h_y}(\phi_{i,j+1} - \phi_{i,j}),$$

$$A_y u_{i+\frac{1}{2},j+\frac{1}{2}} := \tfrac{1}{2}(u_{i+\frac{1}{2},j+1} + u_{i+\frac{1}{2},j}), \quad D_y u_{i+\frac{1}{2},j+\frac{1}{2}} := \tfrac{1}{h_y}(u_{i+\frac{1}{2},j+1} - u_{i+\frac{1}{2},j}). \quad (5.6)$$

The standard 2D discrete Laplacian operator is defined as $\Delta_h : \mathcal{E}_{x \times \overline{y}}^{ew} \cup \mathcal{E}_{\overline{x} \times y}^{ns} \cup \mathcal{C}_{\overline{x} \times \overline{y}} \to \mathcal{E}_{x \times y}^{ew} \cup \mathcal{E}_{x \times y}^{ns} \cup \mathcal{C}_{x \times y}$:

$$\Delta_h u := D_x(d_x u) + d_y(D_y u), \quad \Delta_h v := d_x(D_x v) + D_y(d_y v), \quad \Delta_h \phi := d_x(D_x \phi) + d_y(D_y \phi). \quad (5.7)$$

11

5.1.2 Boundary Conditions

The homogenous Neumann boundary conditions are discretized as follows

$$\phi_{0,j} = \phi_{1,j}, \quad \phi_{N_x,j} = \phi_{N_x+1,j}, \quad j = 0, 1, 2, \cdots, N_y + 1,$$
$$\phi_{i,0} = \phi_{i,1}, \quad \phi_{i,N_y} = \phi_{i,N_y+1}, \quad i = 0, 1, 2, \cdots, N_x + 1. \tag{5.8}$$

We denote it as $\mathbf{n} \cdot \nabla_h \phi|_{\partial V} = 0$.

The homogeneously Dirichlet boundary conditions are discretized as follows

$$u_{\frac{1}{2},j} = u_{N_x+\frac{1}{2},j} = 0, \quad j = 1, 2, \cdots, N_y,$$
$$A_y u_{i+\frac{1}{2},\frac{1}{2}} = A_y u_{i+\frac{1}{2},N_y+\frac{1}{2}} = 0, \quad i = 0, 1, 2, \cdots, N_x,$$
$$v_{i,\frac{1}{2}} = v_{i,N_y+\frac{1}{2}} = 0, \quad j = 1, 2, \cdots, N_x,$$
$$A_x v_{\frac{1}{2},j+\frac{1}{2}} = A_x v_{N_x+\frac{1}{2},j+\frac{1}{2}} = 0, \quad j = 0, 1, 2, \cdots, N_y, \tag{5.9}$$

We denote it as $u_h|_{\partial V} = 0$ and $v_h|_{\partial V} = 0$.

If $f \in \mathcal{V}_{x \times y}$ satisfies homogenous Dirichelet boundary condition, we have

$$f_{\frac{1}{2},j+\frac{1}{2}} = f_{N_x+\frac{1}{2},j+\frac{1}{2}} = f_{i+\frac{1}{2},\frac{1}{2}} = f_{i+\frac{1}{2},N_y+\frac{1}{2}} = 0. \tag{5.10}$$

where $i = 0, 1, 2, \cdots, N_x, j = 0, 1, 2, \cdots, N_y$. We denote is as $f_h|_{\partial V} = 0$.

5.1.3 Inner products and norms

We defined the following inner products for discrete functions

$$(\phi, \psi)_2 := h_x h_y \sum_{i=1}^{N_x} \sum_{j=1}^{N_y} \phi_{i,j} \psi_{i,j}, \quad [u, r]_{ew} := (a_x(ur), 1)_2, \quad [v, w]_{ns} := (a_y(uw), 1)_2,$$
$$(f, g)_{vc} := (a_x(a_y(fg)), 1)_2, \quad (\nabla\phi, \nabla\psi)_h := [D_x(\phi), D_x(\psi)]_{ew} + [D_y(\phi), D_y(\psi)]_{ns}, \tag{5.11}$$

The corresponding norms are defined as follows

$$\|\phi\|_2 := (\phi, \phi)_2^{\frac{1}{2}}, \quad \|u\|_{ew} := [u, u]_{ew}^{\frac{1}{2}}, \quad \|v\|_{ns} := [v, v]_{ns}^{\frac{1}{2}}, \quad \|f\|_{vc} := (f, f)_{vc}^{\frac{1}{2}}. \tag{5.12}$$

For $\phi = \mathcal{C}_{\overline{x} \times \overline{y}}$, we define $\|\nabla\phi\|_2$ as

$$\|\nabla\phi\|_2 := \sqrt{\|D_x\phi\|_{ew}^2 + \|D_y\phi\|_{ns}^2}, \tag{5.13}$$

For the edge-centered velocity vector $\mathbf{v} = (u, v)$, $u \in \mathcal{E}_{x \times \overline{y}}^{ew}, v \in \mathcal{E}_{\overline{x} \times y}^{ns}$, we define $\|\mathbf{v}\|_2, \|\nabla\mathbf{v}\|_2$ as

$$\|\mathbf{v}\|_2 := \sqrt{\|u\|_{ew}^2 + \|v\|_{ns}^2}, \quad \|\nabla\mathbf{v}\|_2 := \sqrt{\|d_x u\|_2^2 + \|D_y u\|_{vc}^2 + \|D_x v\|_{vc}^2 + \|d_y v\|_2^2},$$
$$\|\mathbf{D}\|_2 := \sqrt{\|d_x u\|_2^2 + \tfrac{1}{2}\|D_y u\|_{vc}^2 + \tfrac{1}{2}\|D_x v\|_{vc}^2 + (D_y u, D_x v)_{vc} + \|d_y v\|_2^2},$$
$$(\phi, \mathbf{D} : \mathbf{D})_2 := \tag{5.14}$$
$$\sqrt{(\phi, (d_x u)^2)_2 + \tfrac{1}{2}(A_x(A_y\phi), (D_y u)^2)_{vc} + \tfrac{1}{2}(A_x(A_y\phi), (D_x v)^2)_{vc} + (A_x(A_y\phi)D_y u, D_x v)_{vc} + (\phi, (d_y v)^2)_2}.$$

Where $\mathbf{D} = \frac{1}{2}(\nabla\mathbf{v} + \nabla\mathbf{v}^T)$. From these definitions, we obtain the following lemmas [18]:

Lemma 5.1. (Summation by parts): If $\phi \in \mathcal{C}_{\overline{x} \times \overline{y}}$, $u \in \mathcal{E}_{x \times y}^{ew}$, $v \in \mathcal{E}_{x \times y}^{ns}$, and $u_h|_{\partial V} = 0$ and $v_h|_{\partial V} = 0$, then

$$[A_x \phi, u]_{ew} = (\phi, a_x u)_2, \quad [A_y \phi, v]_{ns} = (\phi, a_y v)_2,$$
$$[D_x \phi, u]_{ew} + (\phi, d_x u)_2 = 0, \quad [D_y \phi, v]_{ns} + (\phi, d_y v)_2 = 0,$$

(5.15)

Lemma 5.2. If $f \in \mathcal{V}_{x \times y}$, and $f_h|_{\partial V} = 0$, $u \in \mathcal{E}_{x \times \overline{y}}^{ew}$, $v \in \mathcal{E}_{\overline{x} \times y}^{ns}$, then

$$[a_y f, u]_{ew} = (f, A_y u)_{vc}, \quad [a_x f, v]_{ns} = (f, A_x v)_{vc}.$$

(5.16)

Lemma 5.3. If $f \in \mathcal{V}_{x \times y}$, $u \in \mathcal{E}_{x \times \overline{y}}^{ew}$, $v \in \mathcal{E}_{\overline{x} \times y}^{ns}$, and $u_h|_{\partial V} = 0$ and $v_h|_{\partial V} = 0$, then

$$[d_y f, u]_{ew} + (f, D_y u)_{vc} = 0, \quad [d_x f, v]_{ns} + (f, D_x v)_{vc} = 0.$$

(5.17)

With these notations and lemmas, we are ready to introduce the fully-discrete numerical scheme in the following section.

5.2 Semi-discrete scheme in time

First, we discretize the governing equations using Crank-Nicolson method in time. We denote

$$\delta_t (\cdot)^{n+1/2} = \tfrac{1}{\Delta t}((\cdot)^{n+1} - (\cdot)^n), \qquad \overline{(\cdot)}^{n+1/2} = \tfrac{1}{2}(3(\cdot)^n - (\cdot)^{n-1}).$$

(5.18)

The second order algorithm is given below.

Algorithm 1.

$$\begin{cases} \delta_t \rho_1^{n+1/2} + \nabla \cdot (\overline{\rho}_1^{n+1/2} \overline{\tfrac{1}{\sqrt{\rho}}}^{n+1/2} \mathbf{u}^{n+1/2}) = \nabla \cdot M_1 \cdot \nabla \mu_1^{n+1/2} - \nabla \cdot M_1 \cdot \nabla \mu_2^{n+1/2}, \\ \delta_t \rho_2^{n+1/2} + \nabla \cdot (\overline{\rho}_2^{n+1/2} \overline{\tfrac{1}{\sqrt{\rho}}}^{n+1/2} \mathbf{u}^{n+1/2}) = -\nabla \cdot M_1 \cdot \nabla \mu_1^{n+1/2} + \nabla \cdot M_1 \cdot \nabla \mu_2^{n+1/2}, \\ \delta_t \mathbf{u}^{n+1/2} + \tfrac{1}{2}(\overline{\tfrac{1}{\sqrt{\rho}}}^{n+1/2} \nabla \cdot (\overline{\mathbf{u}}^{n+1/2} \mathbf{u}^{n+1/2}) + \overline{\mathbf{u}}^{n+1/2} \cdot \nabla(\overline{\tfrac{1}{\sqrt{\rho}}}^{n+1/2} \mathbf{u}^{n+1/2})) = \\ \overline{\tfrac{1}{\sqrt{\rho}}}^{n+1/2} (2\nabla \cdot (\tfrac{1}{Re_s} \mathbf{D}^{n+1/2}) + \nabla(\tfrac{1}{Re_v} \nabla \cdot (\overline{\tfrac{1}{\sqrt{\rho}}}^{n+1/2} \mathbf{u}^{n+1/2})) - \overline{\rho_1}^{n+1/2} \nabla \mu_1^{n+1/2} - \overline{\rho_2}^{n+1/2} \nabla \mu_2^{n+1/2}), \\ \delta_t q_1^{n+1/2} = \overline{\tfrac{\partial q_1}{\partial \rho_1}}^{n+1/2} \delta_t \rho_1^{n+1/2} + \overline{\tfrac{\partial q_1}{\partial \rho_2}}^{n+1/2} \delta_t \rho_2^{n+1/2}, \end{cases}$$

(5.19)

where

$$\mu_1^{n+1/2} = 2q_1^{n+1/2} \overline{\tfrac{\partial q_1}{\partial \rho_1}}^{n+1/2} - \kappa_{\rho_1 \rho_1} \Delta \rho_1^{n+1/2} - \kappa_{\rho_1 \rho_2} \Delta \rho_2^{n+1/2},$$
$$\mu_2^{n+1/2} = 2q_1^{n+1/2} \overline{\tfrac{\partial q_1}{\partial \rho_2}}^{n+1/2} - \kappa_{\rho_1 \rho_2} \Delta \rho_1^{n+1/2} - \kappa_{\rho_2 \rho_2} \Delta \rho_2^{n+1/2},$$
$$\mathbf{D}^{n+1/2} = \tfrac{1}{2}(\nabla(\overline{\tfrac{1}{\sqrt{\rho}}}^{n+1/2} \mathbf{u}^{n+1/2}) + \nabla(\overline{\tfrac{1}{\sqrt{\rho}}}^{n+1/2} \mathbf{u}^{n+1/2})^T),$$
$$\tfrac{1}{Re_s} = \overline{\tfrac{\rho_1}{\rho}}^{n+1/2} \tfrac{1}{Re_{s1}} + \overline{\tfrac{\rho_2}{\rho}}^{n+1/2} \tfrac{1}{Re_{s2}}, \qquad \tfrac{1}{Re_v} = \overline{\tfrac{\rho_1}{\rho}}^{n+1/2} \tfrac{1}{Re_{v1}} + \overline{\tfrac{\rho_2}{\rho}}^{n+1/2} \tfrac{1}{Re_{v2}}.$$

(5.20)

For the scheme, we have the following theorem.

13

Theorem 5.1. *Scheme* (5.19) *is unconditional energy stable, and satisfies the following discrete energy identity*

$$\frac{E^{n+1}-E^n}{\Delta t} = -2(\frac{1}{Re_s}, \mathbf{D}^{n+1/2} : \mathbf{D}^{n+1/2}) - (\frac{1}{Re_v}\nabla \cdot (\overline{\frac{1}{\sqrt{\rho}}}^{n+1/2}\mathbf{u}^{n+1/2}), \nabla \cdot (\overline{\frac{1}{\sqrt{\rho}}}^{n+1/2}\mathbf{u}^{n+1/2}))$$
$$-(\nabla\mu_1^{n+1/2}, \nabla\mu_2^{n+1/2}) \cdot \mathcal{M} \cdot (\nabla\mu_1^{n+1/2}, \nabla\mu_2^{n+1/2})^T < 0, \tag{5.21}$$

Where

$$E^n = \int_V [\frac{1}{2}||\mathbf{u}^n||^2 + (q_1^n)^2 + \frac{1}{2}(\mathbf{p}^n)^T \cdot \mathbf{K}^n \cdot \mathbf{p}^n - A]d\mathbf{x}. \tag{5.22}$$

and $\mathbf{p}^n = (\nabla\rho_1^n, \nabla\rho_2^n)$.

Remark 5.1. We note that a useful identity in the proof of the theorem.

$$(\mathbf{u}^{n+1/2}, \frac{1}{2}(\overline{\frac{1}{\sqrt{\rho}}}^{n+1/2}\nabla \cdot (\overline{\mathbf{u}}^{n+1/2}\mathbf{u}^{n+1/2}) + \overline{\mathbf{u}}^{n+1/2} \cdot \nabla(\overline{\frac{1}{\sqrt{\rho}}}^{n+1/2}\mathbf{u}^{n+1/2}))) = 0. \tag{5.23}$$

Proof: By the definition of E^n, we have

$$\frac{E^{n+1}-E^n}{\Delta t} = \int_V \mathbf{u}^{n+1/2}\delta_t\mathbf{u}^{n+1/2} + 2q_1^{n+1/2}\delta_t q_1^{n+1/2} + \kappa_{\rho_1\rho_1}\nabla\rho^{n+1/2}\delta_t\nabla\rho_1^{n+1/2}$$
$$+\kappa_{\rho_2\rho_2}\nabla\rho_2^{n+1/2}\delta_t\nabla\rho_2^{n+1/2} + \kappa_{\rho_1\rho_2}[\nabla\rho_1^{n+1/2}\delta_t\nabla\rho_2^{n+1/2} + \nabla\rho_2^{n+1/2}\delta_t\nabla\rho_1^{n+1/2}]d\mathbf{x}, \tag{5.24}$$

Taking the inner product of (5.19)-3 with $\mathbf{u}^{n+1/2}$, using identity (5.23), and performing integration by parts, we obtain

$$(\mathbf{u}^{n+1/2}, \delta_t\mathbf{u}^{n+1/2}) = -2(\frac{1}{Re_s}\mathbf{D}^{n+1/2} : \mathbf{D}^{n+1/2}) - (\frac{1}{Re_v}\nabla \cdot (\overline{\frac{1}{\sqrt{\rho}}}^{n+1/2}\mathbf{u}^{n+1/2}), \nabla \cdot (\overline{\frac{1}{\sqrt{\rho}}}^{n+1/2}\mathbf{u}^{n+1/2}))$$
$$-(\mathbf{u}^{n+1/2}, \overline{\frac{1}{\sqrt{\rho}}}^{n+1/2}\overline{\rho_1}^{n+1/2}\nabla\mu_1^{n+1/2} + \overline{\frac{1}{\sqrt{\rho}}}^{n+1/2}\overline{\rho_2}^{n+1/2}\nabla\mu_2^{n+1/2})). \tag{5.25}$$

Taking the inner product of (5.19-4) with $2q_1^{n+\frac{1}{2}}$, using (5.19-1,2), and performing integration by parts, we obtain

$$2(q_1^{n+1/2}, \delta_t q_1^{n+1/2}) = (\overline{\frac{1}{\sqrt{\rho}}}^{n+1/2}\overline{\rho_1}^{n+1/2}, \nabla\mu_1^{n+1/2}) + (\overline{\rho_2}^{n+1/2}\overline{\frac{1}{\sqrt{\rho}}}^{n+1/2}, \nabla\mu_2^{n+1/2})$$
$$-\kappa_{\rho_1\rho_1}\nabla\rho_1^{n+1/2}\delta_t\nabla\rho_1^{n+1/2} - \kappa_{\rho_2\rho_2}\nabla\rho_2^{n+1/2}\delta_t\nabla\rho_2^{n+1/2} - \kappa_{\rho_1\rho_2}[\nabla\rho_1^{n+1/2}\delta_t\nabla\rho_2^{n+1/2} \tag{5.26}$$
$$+\nabla\rho_2^{n+1/2}\delta_t\nabla\rho_1^{n+1/2}] - (\nabla\mu_1^{n+1/2}, \nabla\mu_2^{n+1/2}) \cdot \mathcal{M} \cdot (\nabla\mu_1^{n+1/2}, \nabla\mu_2^{n+1/2})^T.$$

Utilizing (5.24), (5.25) and (5.26), we arrive at the conclusion

$$\frac{E^{n+1}-E^n}{\Delta t} = -2(\frac{1}{Re_s}\mathbf{D}^{n+1/2} : \mathbf{D}^{n+1/2}) - (\frac{1}{Re_v}\nabla \cdot (\overline{\frac{1}{\sqrt{\rho}}}^{n+1/2}\mathbf{u}^{n+1/2}), \nabla \cdot (\overline{\frac{1}{\sqrt{\rho}}}^{n+1/2}\mathbf{u}^{n+1/2}))$$
$$-(\nabla\mu_1^{n+1/2}, \nabla\mu_2^{n+1/2}) \cdot \mathcal{M} \cdot (\nabla\mu_1^{n+1/2}, \nabla\mu_2^{n+1/2})^T \leq 0 \tag{5.27}$$

provided $\mathcal{M} \geq 0$.

14

5.3 Fully Discrete Numerical Scheme

We discretize the semidiscrete equations in (5.19) using the second order finite difference discretization on staggered grids in space to obtain a fully discrete scheme as follows

Algorithm 2.

$$
\begin{cases}
\{\delta_t\rho_1^{n+1/2} + d_x(A_x(\overline{\rho}_1^{n+1/2}\overline{\tfrac{1}{\sqrt{\rho}}}^{n+1/2})u^{n+1/2}) + d_y(A_y(\overline{\rho}_1^{n+1/2}\overline{\tfrac{1}{\sqrt{\rho}}}^{n+1/2})v^{n+1/2}) = \\
M_1\Delta_h\mu_1^{n+1/2} - M_1\Delta_h\mu_2^{n+1/2}\}|_{i,j}, i = 1,\cdots,N_x, j = 1,\cdots,N_y, \\[2mm]
\{\delta_t\rho_2^{n+1/2} + d_x(A_x(\overline{\rho}_2^{n+1/2}\overline{\tfrac{1}{\sqrt{\rho}}}^{n+1/2})u^{n+1/2}) + d_y(A_y(\overline{\rho}_2^{n+1/2}\overline{\tfrac{1}{\sqrt{\rho}}}^{n+1/2})v^{n+1/2}) = \\
-M_1\Delta_h\mu_1^{n+1/2} + M_1\Delta_h\mu_2^{n+1/2}\}|_{i,j}, i = 1,\cdots,N_x, j = 1,\cdots,N_y, \\[2mm]
\{\delta_t u^{n+1/2} + \tfrac{1}{2}(\overline{u}^{n+1/2}D_x(\overline{\tfrac{1}{\sqrt{\rho}}}^{n+1/2}a_x u^{n+1/2}) + A_x(\overline{\tfrac{1}{\sqrt{\rho}}}^{n+1/2}d_x(\overline{u}^{n+1/2}u^{n+1/2}))) \\
+\tfrac{1}{2}(a_x(A_x\overline{v}^{n+1/2}D_y(A_x(\overline{\tfrac{1}{\sqrt{\rho}}}^{n+1/2})u^{n+1/2})) + A_x(\overline{\tfrac{1}{\sqrt{\rho}}}^{n+1/2})d_y(A_y u^{n+1/2}A_x(\overline{v}^{n+1/2})) \\
= g_{v1}\}|_{i+\frac{1}{2},j}, i = 1,\cdots,N_x-1, j = 1,\cdots,N_y, \\[2mm]
\{\delta_t v^{n+1/2} + \tfrac{1}{2}(a_x(A_y\overline{u}^{n+1/2}D_x(A_y(\overline{\tfrac{1}{\sqrt{\rho}}}^{n+1/2})v^{n+1/2})) + A_y(\overline{\tfrac{1}{\sqrt{\rho}}}^{n+1/2})d_x(A_y\overline{u}^{n+1/2}A_x v^{n+1/2})) \\
+\tfrac{1}{2}(\overline{v}^{n+1/2}D_y(\overline{\tfrac{1}{\sqrt{\rho}}}^{n+1/2}a_y v^{n+1/2}) + A_y(\overline{\tfrac{1}{\sqrt{\rho}}}^{n+1/2}d_y(\overline{v}^{n+1/2}v^{n+1/2}))) \\
= g_{v2}\}|_{i,j+\frac{1}{2}}, i = 1,\cdots,N_x, j = 1,\cdots,N_y-1, \\[2mm]
\{\delta_t q_1^{n+1/2} = \overline{\tfrac{\partial q_1}{\partial \rho_1}}^{n+1/2}\delta_t\rho_1^{n+1/2} + \overline{\tfrac{\partial q_1}{\partial \rho_2}}^{n+1/2}\delta_t\rho_2^{n+1/2}\}|_{i,j}, i = 1,\cdots,N_x, j = 1,\cdots,N_y,
\end{cases} \tag{5.28}
$$

where

$$
\begin{aligned}
g_{v1} &= A_x(\overline{\tfrac{1}{\sqrt{\rho}}}^{n+1/2})(2D_x(\tfrac{1}{Re_s^{n+1/2}}d_x(A_x(\overline{\tfrac{1}{\sqrt{\rho}}}^{n+1/2})u^{n+1/2})) + d_y(A_x(A_y\tfrac{1}{Re_s^{n+1/2}})D_y(A_x(\overline{\tfrac{1}{\sqrt{\rho}}}^{n+1/2})u^{n+1/2}))) \\
&+A_x(\overline{\tfrac{1}{\sqrt{\rho}}}^{n+1/2})d_y(A_x(A_y\tfrac{1}{Re_s^{n+1/2}})D_x(A_y(\overline{\tfrac{1}{\sqrt{\rho}}}^{n+1/2})v^{n+1/2})) \\
&+A_x(\overline{\tfrac{1}{\sqrt{\rho}}}^{n+1/2})D_x(\tfrac{1}{Re_v^{n+1/2}}d_x(A_x(\overline{\tfrac{1}{\sqrt{\rho}}}^{n+1/2})u^{n+1/2})) + A_x(\overline{\tfrac{1}{\sqrt{\rho}}}^{n+1/2})D_x(\tfrac{1}{Re_v^{n+1/2}}d_y(A_y(\overline{\tfrac{1}{\sqrt{\rho}}}^{n+1/2})v^{n+1/2})) \\
&-A_x(\overline{\rho_1}^{n+1/2}\overline{\tfrac{1}{\sqrt{\rho}}}^{n+1/2})D_x(\mu_1^{n+1/2}) - A_x(\overline{\rho_2}^{n+1/2}\overline{\tfrac{1}{\sqrt{\rho}}}^{n+1/2})D_x(\mu_2^{n+1/2}),
\end{aligned} \tag{5.29}
$$

$$
\begin{aligned}
g_{v2} &= A_y(\overline{\tfrac{1}{\sqrt{\rho}}}^{n+1/2})(d_x(A_x(A_y\tfrac{1}{Re_s^{n+1/2}})D_x(A_y(\overline{\tfrac{1}{\sqrt{\rho}}}^{n+1/2})v^{n+1/2})) + 2D_y(\tfrac{1}{Re_s^{n+1/2}}d_y(A_y(\overline{\tfrac{1}{\sqrt{\rho}}}^{n+1/2})v^{n+1/2}))) \\
&+A_y(\overline{\tfrac{1}{\sqrt{\rho}}}^{n+1/2})d_x(A_x(A_y\tfrac{1}{Re_s^{n+1/2}})D_y(A_x(\overline{\tfrac{1}{\sqrt{\rho}}}^{n+1/2})u^{n+1/2})) \\
&+A_y(\overline{\tfrac{1}{\sqrt{\rho}}}^{n+1/2})D_y(\tfrac{1}{Re_v^{n+1/2}}d_x(A_x(\tfrac{1}{\sqrt{\rho}})u^{n+1/2})) + A_y(\overline{\tfrac{1}{\sqrt{\rho}}}^{n+1/2})D_y(\tfrac{1}{Re_v^{n+1/2}}d_y(A_y(\overline{\tfrac{1}{\sqrt{\rho}}}^{n+1/2})v^{n+1/2})) \\
&-A_y(\overline{\rho_1}^{n+1/2}\overline{\tfrac{1}{\sqrt{\rho}}}^{n+1/2})D_y(\mu_1^{n+1/2}) - A_y(\overline{\rho_2}^{n+1/2}\overline{\tfrac{1}{\sqrt{\rho}}}^{n+1/2})D_y(\mu_2^{n+1/2}).
\end{aligned} \tag{5.30}
$$

For any time step t_n, $\rho_i^n, \mu_i^n, i = 1, 2$ and q_1^n satisfy discrete homogeneous Neumann boundary conditions (5.8), u^n, v^n satisfy the discrete homogeneous Dirichlet boundary conditions (5.9). The discrete Reynolds numbers are defined as follows

$$
\begin{aligned}
&\{\frac{1}{Re_s^{n+1/2}} = \overline{(\frac{\rho_1}{\rho})}^{n+1/2}\frac{1}{Re_{s1}} + \overline{(\frac{\rho_2}{\rho})}^{n+1/2}\frac{1}{Re_{s2}}\}|_{i,j}, i = 1, \cdots, N_x, j = 1, \cdots, N_y,\\
&\{\frac{1}{Re_v^{n+1/2}} = \overline{(\frac{\rho_1}{\rho})}^{n+1/2}\frac{1}{Re_{v1}} + \overline{(\frac{\rho_2}{\rho})}^{n+1/2}\frac{1}{Re_{v2}}\}|_{i,j}, i = 1, \cdots, N_x, j = 1, \cdots, N_y.
\end{aligned}
\tag{5.31}
$$

Theorem 5.2. *Scheme (5.28) is unconditionally energy stable, and the discrete total energy satisfies the following identity*

$$
\begin{aligned}
\frac{E_h^{n+1}-E_h^n}{\Delta t} &= -2(\frac{1}{Re_s}, \mathbf{D}_h^{n+1/2} : \mathbf{D}_h^{n+1/2})_2 - (\frac{1}{Re_v}tr(\mathbf{D}_h^{n+1/2}), tr(\mathbf{D}_h^{n+1/2}))_2\\
&-M_1(\nabla(\mu_1^{n+1/2} - \mu_2^{n+1/2}), \nabla(\mu_1^{n+1/2} - \mu_2^{n+1/2}))_2 \leq 0,
\end{aligned}
\tag{5.32}
$$

where

$$
\begin{aligned}
E_h^n &= \tfrac{1}{2}[u^n, u^n]_{ew} + \tfrac{1}{2}[v^n, v^n]_{ns} + (q_1^n, q_1^n)_2 - (A, 1)_2\\
&+\tfrac{1}{2}\kappa_{\rho_1\rho_1}(\nabla\rho_1^n, \nabla\rho_1^n)_h + \tfrac{1}{2}\kappa_{\rho_2\rho_2}(\nabla\rho_2^n, \nabla\rho_2^n)_h + \kappa_{\rho_1\rho_2}(\nabla\rho_1^n, \nabla\rho_2^n)_h.
\end{aligned}
\tag{5.33}
$$

and

$$
\mathbf{D}_h^{n+1/2} = \begin{pmatrix} d_x(A_x(\overline{\frac{1}{\sqrt{\rho}}}^{n+1/2})u^{n+1/2})) & \tfrac{1}{2}S \\ \tfrac{1}{2}S & d_y(A_y(\overline{\frac{1}{\sqrt{\rho}}}^{n+1/2})v^{n+1/2})) \end{pmatrix}
\tag{5.34}
$$

where $S = D_x(A_y(\overline{\frac{1}{\sqrt{\rho}}}^{n+1/2})v^{n+1/2}) + D_y(A_x(\overline{\frac{1}{\sqrt{\rho}}}^{n+1/2})u^{n+1/2}))$.

Remark 5.2. We note that using lemmas (5.1)-(5.3), we could obtain identities as follows

$$
\begin{aligned}
&(u^{n+1/2}, \tfrac{1}{2}(\overline{u}^{n+1/2}D_x(\overline{\frac{1}{\sqrt{\rho}}}^{n+1/2}a_x u^{n+1/2}) + A_x(\overline{\frac{1}{\sqrt{\rho}}}^{n+1/2}d_x(\overline{u}^{n+1/2}u^{n+1/2})))\\
&+\tfrac{1}{2}(a_x(A_x\overline{v}^{n+1/2}D_y(A_x(\overline{\frac{1}{\sqrt{\rho}}}^{n+1/2})u^{n+1/2})) + A_x(\overline{\frac{1}{\sqrt{\rho}}}^{n+1/2})d_y(A_y u^{n+1/2}A_x(\overline{v}^{n+1/2})) = 0,
\end{aligned}
\tag{5.35}
$$

$$
\begin{aligned}
&(v^{n+1/2}, \tfrac{1}{2}(a_x(A_y\overline{u}^{n+1/2}D_x(A_y(\overline{\frac{1}{\sqrt{\rho}}}^{n+1/2})v^{n+1/2})) + A_y(\overline{\frac{1}{\sqrt{\rho}}}^{n+1/2})d_x(A_y\overline{u}^{n+1/2}A_x v^{n+1/2}))\\
&+\tfrac{1}{2}(\overline{v}^{n+1/2}D_y(\overline{\frac{1}{\sqrt{\rho}}}^{n+1/2}a_y v^{n+1/2}) + A_y(\overline{\frac{1}{\sqrt{\rho}}}^{n+1/2}d_y(\overline{v}^{n+1/2}v^{n+1/2})))) = 0.
\end{aligned}
$$

Proof: It follows from the definition of E_h^n that

$$
\begin{aligned}
\frac{E_h^{n+1}-E_h^n}{\Delta t} &= [\frac{u^{n+1}+u^n}{2}, \frac{u^{n+1}-u^n}{\Delta t}]_{ew} + [\frac{v^{n+1}+v^n}{2}, \frac{v^{n+1}-v^n}{\Delta t}]_{ns} + 2(\frac{q_1^{n+1}+q_1^n}{2}, \frac{q_1^{n+1}-q_1^n}{\Delta t})_2\\
&+\kappa_{\rho_1\rho_1}(\frac{\nabla\rho_1^{n+1}+\nabla\rho_1^n}{2}, \frac{\nabla\rho_1^{n+1}-\nabla\rho_1^n}{\Delta t})_h + \kappa_{\rho_2\rho_2}(\frac{\nabla\rho_2^{n+1}+\nabla\rho_2^n}{2}, \frac{\nabla\rho_2^{n+1}-\nabla\rho_2^n}{\Delta t})_h\\
&+\kappa_{\rho_1\rho_2}[(\frac{\nabla\rho_1^{n+1}+\nabla\rho_1^n}{2}, \frac{\nabla\rho_2^{n+1}-\nabla\rho_2^n}{\Delta t})_h + (\frac{\nabla\rho_2^{n+1}+\nabla\rho_2^n}{2}, \frac{\nabla\rho_1^{n+1}-\nabla\rho_1^n}{\Delta t})_h]
\end{aligned}
\tag{5.36}
$$

16

Taking the inner product of (5.28-3,4) with $u^{n+1/2}, v^{n+1/2}$ respectively and using identify (5.35), we obtain

$$
\begin{aligned}
&[\tfrac{u^{n+1}+u^n}{2}, \tfrac{u^{n+1}-u^n}{\Delta t}]_{ew} + [\tfrac{v^{n+1}+v^n}{2}, \tfrac{v^{n+1}-v^n}{\Delta t}]_{ns} \\
&= -2(\tfrac{1}{Re_s}, \mathbf{D}_h^{n+1/2} : \mathbf{D}_h^{n+1/2})_2 - (\tfrac{1}{Re_v} tr(\mathbf{D}_h^{n+1/2}), tr(\mathbf{D}_h^{n+1/2}))_2 \\
&\quad -[u^{n+1/2}, A_x(\overline{\rho_1}^{n+1/2}\overline{\tfrac{1}{\sqrt{\rho}}}^{n+1/2})D_x(\mu_1^{n+1/2}) + A_x(\overline{\rho_2}^{n+1/2}\overline{\tfrac{1}{\sqrt{\rho}}}^{n+1/2})D_x(\mu_2^{n+1/2})]_{ew} \\
&\quad -[v^{n+1/2}, A_y(\overline{\rho_1}^{n+1/2}\overline{\tfrac{1}{\sqrt{\rho}}}^{n+1/2})D_y(\mu_1^{n+1/2}) + A_y(\overline{\rho_2}^{n+1/2}\overline{\tfrac{1}{\sqrt{\rho}}}^{n+1/2})D_y(\mu_2^{n+1/2})]_{ns},
\end{aligned}
\tag{5.37}
$$

Where we used lemmas (5.1) and (5.3). Taking the inner product of (5.28-5) with $2q_1^{n+1/2}$, and performing integration by parts, we obtain

$$
\begin{aligned}
&2(\tfrac{q_1^{n+1}+q_1^n}{2}, \tfrac{q_1^{n+1}-q_1^n}{\Delta t})_2 = -M_1(\nabla(\mu_1^{n+1/2} - \mu_2^{n+1/2}), \nabla(\mu_1^{n+1/2} - \mu_2^{n+1/2}))_h \\
&+[A_x(\overline{\rho_1}^{n+1/2}\overline{\tfrac{1}{\sqrt{\rho}}}^{n+1/2})u^{n+1/2}, D_x(\mu_1^{n+1/2})]_{ew} + [A_y(\overline{\rho_1}^{n+1/2}\overline{\tfrac{1}{\sqrt{\rho}}}^{n+1/2})v^{n+1/2}, D_y(\mu_1^{n+1/2})]_{ns} \\
&+[A_x(\overline{\rho_2}^{n+1/2}\overline{\tfrac{1}{\sqrt{\rho}}}^{n+1/2})u^{n+1/2}, D_x(\mu_2^{n+1/2})]_{ew} + [A_y(\overline{\rho_2}^{n+1/2}\overline{\tfrac{1}{\sqrt{\rho}}}^{n+1/2})v^{n+1/2}, D_y(\mu_2^{n+1/2})]_{ns} \\
&-\kappa_{\rho_1\rho_1}(\tfrac{\nabla\rho_1^{n+1}+\nabla\rho_1^n}{2}, \tfrac{\nabla\rho_1^{n+1}-\nabla\rho_1^n}{\Delta t})_h - \kappa_{\rho_2\rho_2}(\tfrac{\nabla\rho_2^{n+1}+\nabla\rho_2^n}{2}, \tfrac{\nabla\rho_2^{n+1}-\nabla\rho_2^n}{\Delta t})_h \\
&-\kappa_{\rho_1\rho_2}[(\tfrac{\nabla\rho_1^{n+1}+\nabla\rho_1^n}{2}, \tfrac{\nabla\rho_2^{n+1}-\nabla\rho_2^n}{\Delta t})_h + (\tfrac{\nabla\rho_2^{n+1}+\nabla\rho_2^n}{2}, \tfrac{\nabla\rho_1^{n+1}-\nabla\rho_1^n}{\Delta t})_h],
\end{aligned}
\tag{5.38}
$$

where we used lemma (5.1). Combining (5.36), (5.37) and (5.38), we obtain

$$
\begin{aligned}
\tfrac{E_h^{n+1}-E_h^n}{\Delta t} &= -2(\tfrac{1}{Re_s}, \mathbf{D}_h^{n+1/2} : \mathbf{D}_h^{n+1/2})_2 - (\tfrac{1}{Re_v} tr(\mathbf{D}_h^{n+1/2}), tr(\mathbf{D}_h^{n+1/2}))_2 \\
&\quad -M_1(\nabla(\mu_1^{n+1/2} - \mu_2^{n+1/2}), \nabla(\mu_1^{n+1/2} - \mu_2^{n+1/2}))_2 \leq 0,
\end{aligned}
\tag{5.39}
$$

provided $M_1 \geq 0$. Having established unconditional energy stability, we now turn to the solvability issue of the linear system of equations.

5.4 Unique Solvability of the Fully Discrete, Linear Numerical Scheme

The linear system resulting from scheme (5.28) can be written into

$$
\mathcal{A} \cdot X = \mathcal{G},
\tag{5.40}
$$

where $\mathcal{A}$ is the coefficient matrix of the system given in Appendix, $X := (\mu_1, \mu_2, u, v, q_1, \rho_1, \rho_2)$ is the solution of the linear system and the right hand term $\mathcal{G} = (g_1, g_2, g_3, g_4, g_5, g_6, g_7)^T$ denotes all the terms at the nth time step.

Theorem 5.3. *Linear system (5.28) admits a unique solution.*
Proof: To prove the well-posedness of the system (5.28), we only need to prove the corresponding homogeneous system admits only the zero solution. We assume that there is a solution $X = (\mu_1, \mu_2, u, v, q_1, \rho_1, \rho_2)$ such that $\mathcal{A} \cdot X = 0$. Using (8.1), we have

$$
\begin{aligned}
0 = (\mathcal{A} \cdot X, X)_2 &= M_1(\nabla(\mu_1 - \mu_2), \nabla(\mu_1 - \mu_2))_2 + \tfrac{2}{\Delta t}[u, u]_{ew} + \tfrac{2}{\Delta t}[v, v]_{ns} + \tfrac{4}{\Delta t}(q_1, q_1)_2 \\
&+2(\tfrac{1}{Re_s}, \mathbf{D}_h : \mathbf{D}_h)_2 + (\tfrac{1}{Re_v} tr(\mathbf{D}_h), tr(\mathbf{D}_h))_2 + \tfrac{2}{\Delta t}[\kappa_{\rho_1\rho_1}(\nabla\rho_1, \nabla\rho_1)_h + \kappa_{\rho_2\rho_2}(\nabla\rho_2, \nabla\rho_2)_h] \\
&+\tfrac{4}{\Delta t}\kappa_{\rho_1\rho_2}(\nabla\rho_1, \nabla\rho_2)_h \geq C((\nabla\rho_1, \nabla\rho_2)_h + (\nabla\rho_2, \nabla\rho_2)_h + [u, u]_{ew} + [v, v]_{ns} + \|q_1\|_2^2),
\end{aligned}
\tag{5.41}
$$

where we used $\mathbf{K} > 0$, C is a positive constant and $\mathbf{D}_h$ is defined in (8.3). Thus, we obtain

$$D_x \rho_1 = D_y \rho_1 = 0, \quad D_x \rho_1 = D_y \rho_2 = 0, \quad u = v = 0, \quad q_1 = 0, \tag{5.42}$$

Based on linear system (8.1), we have

$$\mu_1 = \mu_2 = 0, \quad \rho_1 = \rho_2 = 0, \tag{5.43}$$

i.e. $X = \mathbf{0}$. Thus, linear system (5.28) admits an unique solution.

Remark 5.3. A second order in time, energy stable BDF scheme can be developed as well, which will not be presented here.

6 Numerical results and discussions

6.1 Accuracy Test

We conduct a mesh refinement test to verify the convergence rate of the numerical scheme by considering (3.2) with a double-well bulk free energy

$$h(\rho_1, \rho_2, T) = \rho_1^2 (\rho_1 - 1)^2 + \rho_2^2 (\rho_2 - 1)^2, \tag{6.1}$$

in a rectangular domain $\Omega = [0, 1] \times [0, 1]$. We use the following initial conditions

$$\rho_1(x, y, t = 0) = 0.5 + 0.01 cos(2\pi x), \quad \rho_2(x, y, t = 0) = 0.5 - 0.01 cos(2\pi x), \quad \mathbf{v} = (0, 0). \tag{6.2}$$

We denote the number of spatial grids as $N_x = N_y = N$, the time step as Δt. To test the convergence rate in time, we first fix $N = 256$ and vary the time step from 4×10^{-3} to 0.125×10^{-3} to calculate the l_2 norm of the difference between the numerical solutions obtained using consecutive step sizes at $T = 0.1$, i.e. $\|(\cdot)_{\Delta t}(T) - (\cdot)_{2\Delta t}(T)\|_2$. Then, we fix time step $\Delta t = 10^{-4}$, vary the spatial grid number from 8 to 256 and calculate the l_2 norm of the difference between the numerical solutions obtained using consecutive grid sizes at $T = 0.1$, i.e. $\|(\cdot)_h(T) - (\cdot)_{2h}(T)\|_2$. In both space and time, we calculate the convergence rate using $p = log_2 \left(\frac{\|(\cdot)_{2h}(T) - (\cdot)_{4h}(T)\|_2}{\|(\cdot)_h(T) - (\cdot)_{2h}(T)\|_2} \right)$, where h is the mesh size in time or space. The refinement results are tabulated in Table 6.1 and Table 6.2, respectively. We observe that the proposed scheme is indeed second-order accurate in both time and space for all variables.

6.2 Phase Separation in binary compressible viscous fluids

To demonstrate stability and efficiency of the new scheme, we simulate phase separation dynamics using system (3.2) with the Flory-Huggins mixing energy

$$h(\rho_1, \rho_2, T) = \frac{k_B T}{m} \rho \left(\frac{1}{N_1} \frac{\rho_1}{\rho} ln \frac{\rho_1}{\rho} + \frac{1}{N_2} \frac{\rho_2}{\rho} ln \frac{\rho_2}{\rho} + \chi \frac{\rho_1 \rho_2}{\rho^2} \right), \tag{6.3}$$

18

Δt	$\|(\rho_1)_{\Delta t} - (\rho_1)_{2\Delta t}\|_2$	order	$\|(\rho_2)_{\Delta t} - (\rho_2)_{2\Delta t}\|_2$	order	$\|(\mathbf{u})_{\Delta t} - (\mathbf{u})_{2\Delta t}\|_2$	order
4×10^{-3}						
2×10^{-3}	0.5237×10^{-8}		0.5240×10^{-8}		0.1498×10^{-7}	
1×10^{-3}	0.1348×10^{-8}	1.96	0.1349×10^{-8}	1.96	0.3806×10^{-8}	1.98
0.5×10^{-3}	0.3425×10^{-9}	1.98	0.3428×10^{-9}	1.98	0.9594×10^{-9}	1.99
0.25×10^{-3}	0.8644×10^{-10}	1.99	0.8651×10^{-10}	1.99	0.2435×10^{-9}	1.98
0.125×10^{-3}	0.2129×10^{-10}	2.02	0.2130×10^{-10}	2.02	0.5779×10^{-10}	2.08

Table 6.1: Temporal refinement result for all variables. The model parameter values are chosen as $Re_s = 100, Re_v = 300, M_1 = 10^{-7}$, $\kappa_{\rho_1\rho_1} = \kappa_{\rho_2\rho_2} = 10^{-4}$, $\kappa_{\rho_1\rho_2} = \kappa_{\rho_2\rho_1} = 0$.

N	$\|(\rho_1)_h - (\rho_1)_{2h}\|_2$	order	$\|(\rho_2)_h - (\rho_2)_{2h}\|_2$	order	$\|(\mathbf{u})_h - (\mathbf{u})_{2h}\|_2$	order
8						
16	0.2281×10^{-5}		0.2282×10^{-5}		0.2676×10^{-7}	
32	0.3417×10^{-6}	1.74	0.3421×10^{-6}	1.74	0.3487×10^{-8}	1.85
64	0.4452×10^{-7}	1.94	0.4457×10^{-7}	1.93	0.4607×10^{-9}	1.88
128	0.5623×10^{-8}	1.98	0.5631×10^{-8}	1.99	0.5898×10^{-10}	1.95
256	0.7050×10^{-9}	2.00	0.7059×10^{-9}	2.00	0.7444×10^{-11}	1.98

Table 6.2: Spatial refinement result for all variables. The model parameter values are chosen as $Re_s = 1, Re_v = 3, M_1 = 10^{-3}$, $\kappa_{\rho_1\rho_1} = \kappa_{\rho_2\rho_2} = 10^{-4}$, $\kappa_{\rho_1\rho_2} = \kappa_{\rho_2\rho_1} = 0$.

(a) Flory-Huggins mixing energy density function with respect to $\frac{\rho_1}{\rho}$
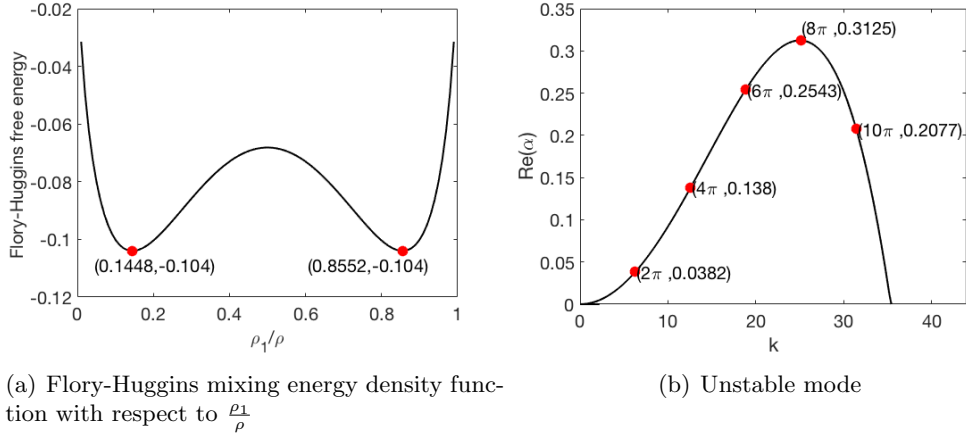
(b) Unstable mode

Figure 6.1: (a) Flory-Huggins mixing energy density function with respect to the mass density fraction $\frac{\rho_1}{\rho}$ at the chosen parameter values. The two minima are labeled by dots in the curve. (b) The unstable mode with parameter values: $N_1 = N_2 = 1, \chi = 2.5, M_1 = 10^{-3}, Re_s = 100, Re_v = 300, \kappa_{\rho_1\rho_1} = \kappa_{\rho_2\rho_2} = 0.0004, \kappa_{\rho_1\rho_2} = 0$.

where we choose the characteristic scales so that $\frac{k_B T}{m} = 1$ in the simulation, N_1, N_2 are the polymerization indices and χ is the mixing coefficient, which are given in the simulation by

$$N_1 = N_2 = 1, \qquad \chi = 2.5. \tag{6.4}$$

The plot of this energy density with the chosen parameter values as a function of $\frac{\rho_1}{\rho}$ is shown in 6.1-(a). The other dimensionless model parameters are chosen as follows

$$M_1 = 10^{-3}, \quad Re_s = 100, \quad Re_v = 300, \quad \kappa_{\rho_1\rho_1} = \kappa_{\rho_2\rho_2} = 4 \times 10^{-4}, \quad \kappa_{\rho_1\rho_2} = 0. \tag{6.5}$$

In order to identify the spinodal decomposition that drives the phase separation in the binary polymer blend, we conduct a simple linear stability analysis on the hydrodynamic phase field model. We note that this compressible model admits a family of constant solutions:

$$\mathbf{v} = \mathbf{0}, \quad \rho_1 = \rho_1^0, \quad \rho_2 = \rho_2^0, \tag{6.6}$$

where ρ_1^0, ρ_2^0 are constants. We perturb the constant solutions with a normal mode as follows:

$$\mathbf{v} = \epsilon e^{\alpha t + i\mathbf{k} \cdot \mathbf{x}} \mathbf{v}^c, \quad \rho_1 = \rho_1^0 + \epsilon e^{\alpha t + i\mathbf{k} \cdot \mathbf{x}} \rho_1{}^c, \quad \rho_2 = \rho_2^0 + \epsilon e^{\alpha t + i\mathbf{k} \cdot \mathbf{x}} \rho_2{}^c, \tag{6.7}$$

where ϵ is a small parameter, representing the magnitude of the perturbation, and $\mathbf{v}^c, \rho_1^c, \rho_2^c$ are constants, α is the growth rate, and $\mathbf{k}$ is the wave number of the perturbation. Without loss of generality, we limit our study to 1 dimensional perturbation in $\mathbf{k}$ in the (x, y) plane. Substituting these perturbations into the equations in (3.2) and truncating the equations at order $O(\epsilon)$, we

20

obtain the linearized equations. The dispersion equation of the linearized equation system of the compressible model [58] is given by an algebraic equation of α:

$$
\begin{aligned}
&(\eta^0 k^2 + \alpha \rho^0)\{\alpha^3 \rho_0 + \alpha^2 k^2 [\eta + \rho^0 M_1(h_{\rho_1 \rho_1} + \kappa_{\rho_1 \rho_1} k^2) + \rho^0 M_1(h_{\rho_2 \rho_2} + \kappa_{\rho_2 \rho_2} k^2)] \\
&-\alpha^2 k^2 [2\rho^0 M_1(h_{\rho_1 \rho_2} + \kappa_{\rho_1 \rho_2} k^2)] + \alpha[\mathbf{p}^T \cdot \mathbf{C} \cdot \mathbf{p} + \mathbf{p}^T \cdot \mathbf{K} \cdot \mathbf{p} k^2] k^2 \\
&+\alpha \eta M_1[(h_{\rho_1 \rho_1} + \kappa_{\rho_1 \rho_1} k^2) + (h_{\rho_2 \rho_2} + \kappa_{\rho_2 \rho_2} k^2) - 2(h_{\rho_1 \rho_2} + \kappa_{\rho_1 \rho_2} k^2)] k^4 \\
&+k^4 M_1(\rho_1^0 + \rho_2^0)^2 [(h_{\rho_1 \rho_1} + \kappa_{\rho_1 \rho_1} k^2)(h_{\rho_2 \rho_2} + \kappa_{\rho_2 \rho_2} k^2) - (h_{\rho_1 \rho_2} + \kappa_{\rho_1 \rho_2} k^2)^2] \} = 0,
\end{aligned}
\tag{6.8}
$$

where $\eta = 2\eta^0 + \bar{\eta}^0$, $\mathbf{p} = (\rho_1^0, \rho_2^0)^T$. In the following, we set $\rho_1^0 = \rho_2^0 = 0.5$. $\mathbf{K}$ is the coefficient matrix of the conformational entropy and $\mathbf{C}$ is the Hessian of bulk energy $h(\rho_1, \rho_2, T)$ with respect to ρ_1 and ρ_2,

$$
\mathbf{K} = \begin{pmatrix} \kappa_{\rho_1 \rho_1} & \kappa_{\rho_1 \rho_2} \\ \kappa_{\rho_1 \rho_2} & \kappa_{\rho_2 \rho_2} \end{pmatrix}, \mathbf{C} = \begin{pmatrix} h_{\rho_1 \rho_1} & h_{\rho_1 \rho_2} \\ h_{\rho_1 \rho_2} & h_{\rho_2 \rho_2} \end{pmatrix}.
\tag{6.9}
$$

Obviously, $\alpha = -\frac{\eta^0}{\rho^0} k^2 < 0$ is a solution of the dispersion equation (6.8), which contributes a stable mode. To resolve the other modes, we use numerical calculations. Based on the model parameters listed above, we obtain only one unstable mode, shown in Figure 6.1-(b). This unstable mode is dominated by the mixing energy of the model, independent of hydrodynamics of the model. Next, we will numerically simulate phase separation phenomena due to the unstable perturbation on the constant steady state without and with hydrodynamics to show how hydrodynamics can affect the path of phase separation and its outcome.

6.2.1 Phase separation without hydrodynamics

Based on unstable mode shown in Figure (6.1-b), we add a 1D perturbation with wave number $k = 10\pi$ to the steady state and observe its ensuing nonlinear dynamics. Since the eigenvector corresponding to the unstable mode shown in Figure (6.1-b) is $(\rho_1^c, \rho_2^c) = (1, -1)$, we impose the initial conditions specifically as follows

$$
\rho_1(x, y, t = 0) = 0.5 + 0.005 \times cos(10\pi y), \qquad \rho_2(x, y, t = 0) = 0.5 - 0.005 \times cos(10\pi y). \tag{6.10}
$$

Since $\rho_1 + \rho_2 = 1$ in the thermodynamic model without hydrodynamics, we show the phase behavior of ρ_1 only. The time evolution of ρ_1 at a few selected times are depicted in Figure 6.2. Firstly, we observe that the growth rate of the numerical solutions ρ_1 near the equilibrium state is $\alpha = 0.2077$, which matches with the linear stability analysis result shown in Figure (6.1-b). In the long-time behavior, we observe that ρ_1 develops small-scale structures and then coarsens to large-scale structures eventually. In Figure 6.2, we show numerical solutions at several time slots and the corresponding total energy up to $t = 15000$. The system goes through three coarsening events which are captured by the phase morphology at different times shown as well as the total energy evolution in Figure 6.2. The outcome at the end of the computation is a four-band structure.

21

(a) ρ_1 at t = 0   (b) ρ_1 at t = 300   (c) ρ_1 at t = 2000   (d) ρ_1 at t = 15000

(e) Total Energy

(f) Difference of total mass of the component 1 with its initial total mass

(g) Difference of total mass of the component 2 with its initial total mass
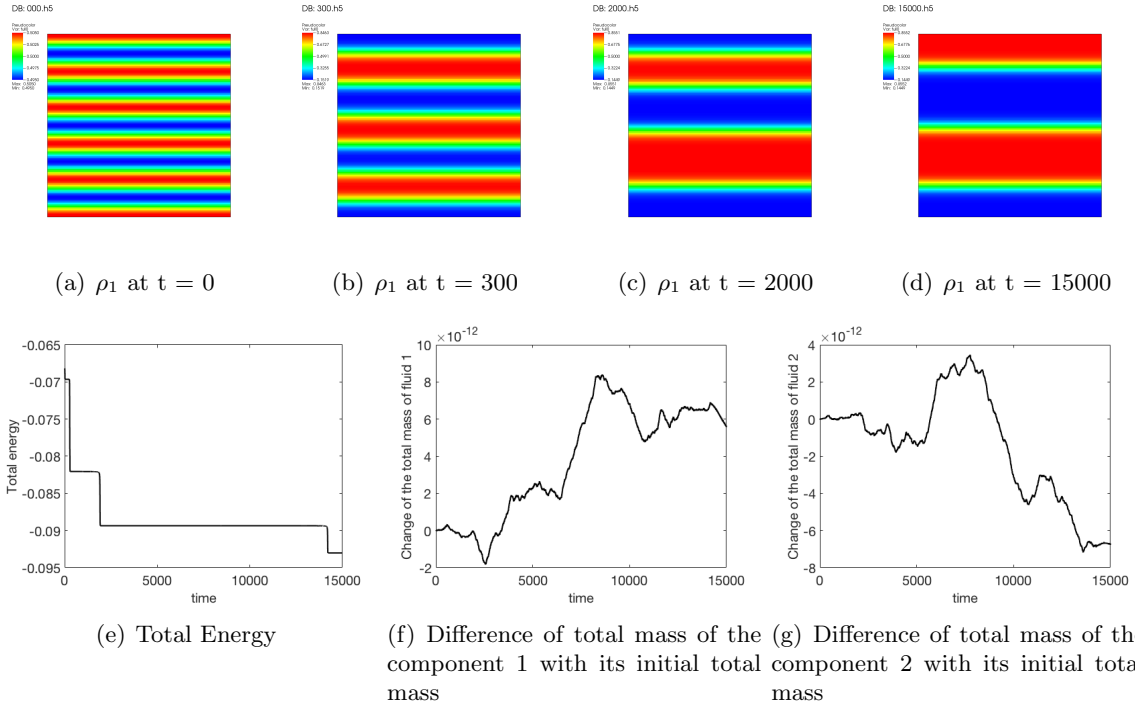
Figure 6.2: (a-d) Snapshots of ρ_1 at different times as solutions of system (3.2) with the Flory-Huggins mixing energy (6.3) without hydrodynamics. (e) The total free energy of system (3.2). Two major coarsening events bring the phase of the binary system into the final state shown in (d). ρ_2 is given by $1 - \rho_1$. The total mass of both phases are conserved as shown in (f-g).

6.2.2　Phase separation with hydrodynamics

When hydrodynamics is coupled with the thermodynamical phase evolution, its role must show up somewhere. Here, we investigate how hydrodynamic impact on phase separation dynamics. Since the eigenvector corresponding to the unstable mode shown in Figure (6.1-b) is $(\rho_1^c, \rho_2^c) = (1, -1, 0)$, we adopt the same initial conditions for ρ_1 and ρ_2 as before and a zero velocity condition:

$$\rho_1(x,y,0) = 0.5 + 0.005 \times cos(10\pi y), \quad \rho_2(x,y,0) = 0.5 - 0.005 \times cos(10\pi y), \quad \mathbf{v}(x,y,0) = (0,0) \quad (6.11)$$

When hydrodynamics is considered, the local total mass density ρ is no longer spatially homogeneous anymore. However, phase separation goes on as shown in Figure 6.3 and Figure 6.4. In Figure 6.3, we observe that the total energy of the system is dissipative and the total mass of component 1 and 2 are conserved in the domain globally. The velocity field in the domain is plotted at the selected times. Some vorticities form and disperse eventually as the phase morphology approaches a steady state. The induced nontrivial velocity field promotes the transport of materials and mixing across the domain leading to a two-band structure phase morphology eventually, which is a global energy stable state. In contrast, the final phase morphology developed in the phase separation without hydrodynamics may have only reached a local energy stable state, which can be explained by the comparison of the total energy evolutions shown in Figure (6.2-e) and Figure (6.3-i), respectively. This tells us that hydrodynamics indeed changes local densities, the path of phase evolution and even the final energy steady states of fluid mixtures. This is alarming, indicating that hydrodynamic effects are instrumental in determining the correct spatial phase diagram for the binary fluid mixture. The total energy in the solution with hydrodynamics is smaller than that without it. So, hydrodynamics in a binary compressible fluid flow promotes fluid mixing and thereby speeds up phase separation.

6.3　Dynamics of gas-liquid Mixtures

The compressible fluid model has many applications in the petroleum industry, where mixtures of non-hydrocarbons and hydrocarbons are abundant, such as in petroleum reservoirs or natural gas pipelines. Understanding their thermodynamic and hydrodynamic properties can help one to improve petroleum quality and yield significantly.

In the past, several equations of state had been developed to describe the relation among state variables (e.g. the volume, pressure and temperature) under a given set of physical conditions for compressible fluids. The Peng-Robinson equation of state (PR-EOS) [36] is one of the popular ones, which has been successfully applied to thermodynamic and volumetric calculations in both industries and academics. Specifically, PR-EOS provides a reasonable accuracy near the critical point, which makes it a good choice for gas-condensate systems in the petroleum industry. For this reason, we adopt it in a hydrocarbon mixture of methane and n-decane to show the performance of our model and numerical scheme in simulating hydrodynamics of the hydrocarbon mixtures. Many properties of the mixture can be studied by our mathematical model, such as mass adsorption of one component in the mixture on the interface between two phases near the equilibrium state, surface tension and even verification of mixing rules in the mixture. In this example, we will focus on hydrodynamics of a hydrocarbon mixture with an unstable gas-liquid interface and study the

(a) ρ_1 at t = 0 (b) ρ_1 at t = 50 (c) ρ_1 at t = 100 (d) ρ_1 at t = 150

(e) ρ_1 at t = 200 (f) ρ_1 at t = 400 (g) ρ_1 at t = 600 (h) ρ_1 at t = 1400

(i) Total Energy

(j) Difference of total mass of the component 1 with its initial total mass

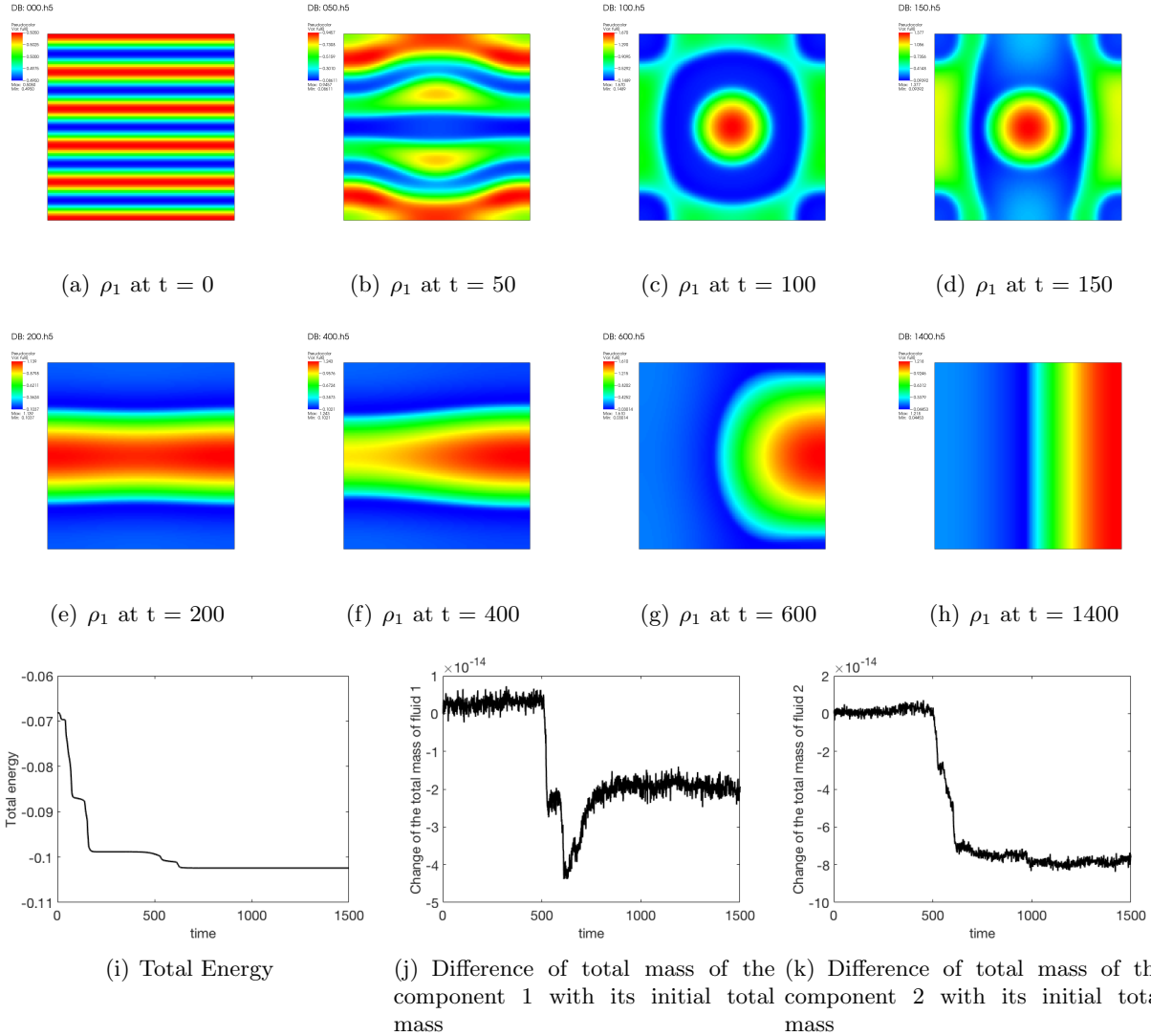(k) Difference of total mass of the component 2 with its initial total mass

Figure 6.3: (a-h) Snapshots of ρ_1 at different times as a solution of system (3.2) with the Flory-Huggins mixing energy (6.3) and hydrodynamic interaction. (i) Total energy of the system (3.2) with the Flory-Huggins bulk free energy (6.3); (j, k) Difference of the total mass of component 1 and 2 compared with the initial mass, indicating mass conservation of both phases in the simulation.

24

(a) ρ_2 at t = 0   (b) ρ_2 at t = 50   (c) ρ_2 at t = 100   (d) ρ_2 at t = 150

(e) ρ_2 at t = 200   (f) ρ_2 at t = 400   (g) ρ_2 at t = 600   (h) ρ_2 at t = 1400

(i) $\mathbf{v}$ at t = 0   (j) $\mathbf{v}$ at t = 50   (k) $\mathbf{v}$ at t = 100   (l) $\mathbf{v}$ at t = 150

(m) $\mathbf{v}$ at t = 200   (n) $\mathbf{v}$ at t = 400   (o) $\mathbf{v}$ at t = 600   (p) $\mathbf{v}$ at t = 1400
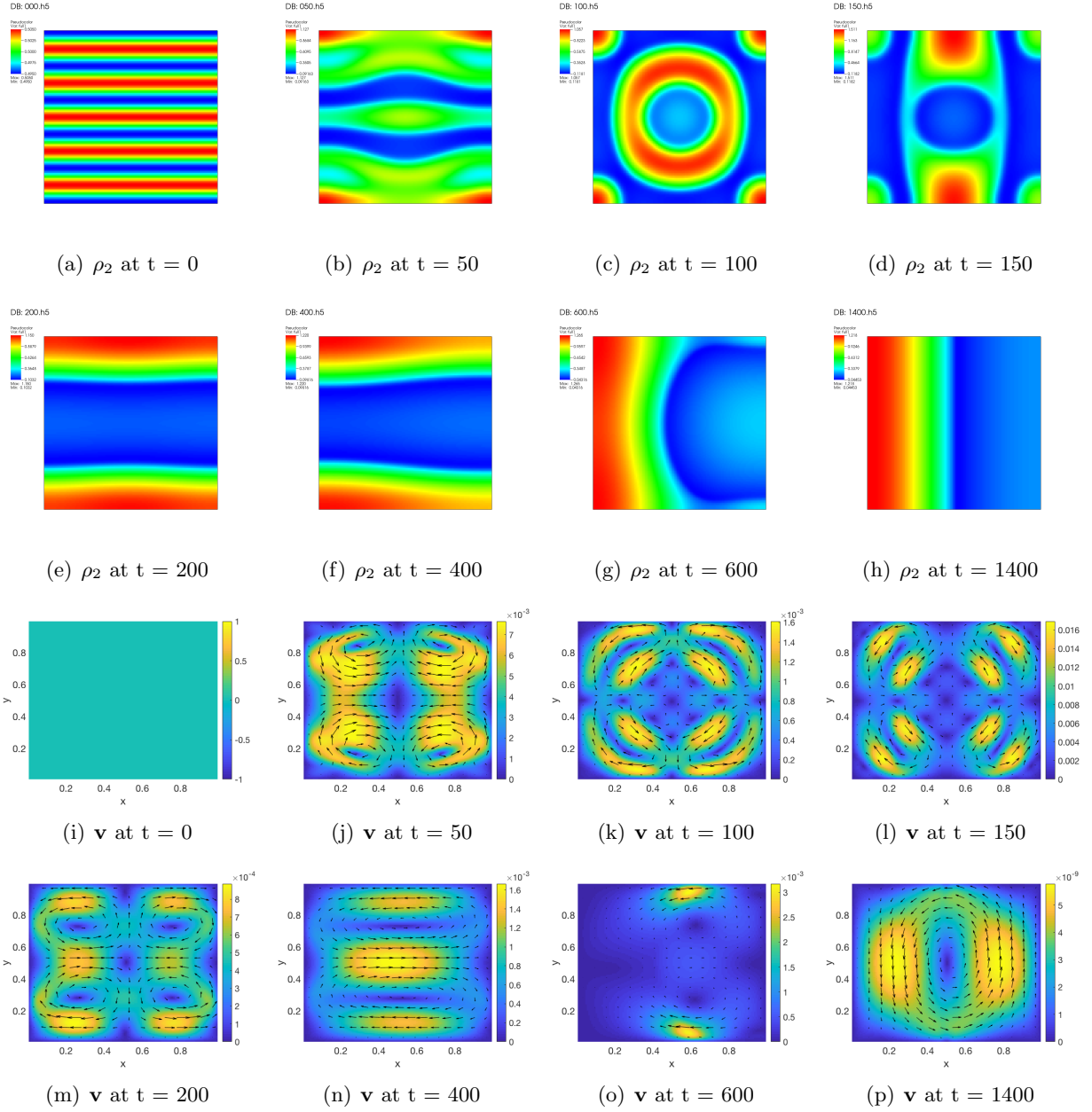
Figure 6.4: (a-h) Snapshots of ρ_2 at different times as a solution of system (3.2) with the Flory-Huggins mixing energy given in (6.3) and hydrodynamic interaction. (i-p) Snapshots for velocity field $\mathbf{v} = (v_1, v_2)$ at different times. Weak flows are present due to hydrodynamic effect during the phase evolution. The nontrivial velocity leads to different phase morphology in the end compared to the case without hydrodynamic interaction at the end of our simulation.

25

Table 6.3: Dimensional critical parameters

Symbol	$T_c(K)$	$P_c(MPa)$	w	m $(kg \cdot mol^{-1})$
n-decane $(C_{10}H_{22})$	617.7	2.103	0.4884	0.14228
methane (CH_4)	190.564	4.5992	0.01142	0.0160428

mass adsorption phenomena at the interface from the point of view of the free energy near an equilibrium state.

The free energy density function derived from PR-EOS reads

$$f = f_b + h(\mathbf{n}, T), \tag{6.12}$$

where $f_b = \frac{1}{2}\sum_{i,j=1}^N c_{i,j}\nabla n_i \cdot \nabla n_j$ is the conformational energy. The bulk free energy density function $h(\mathbf{n}, T)$ is given in (2.22).

Remark 6.1. Since f^{ideal} changes rapidly near the origin which may introduce singularity in numerical simulations, we regularize this term near the origin as follows

$$f^{ideal} = \begin{cases} RTn_i(ln(\epsilon) - 1) + RT(\frac{1}{2\epsilon}n_i^2 - \frac{\epsilon}{2}), & if \quad n_i < \epsilon, \\ RTn_i(ln(n_i) - 1), \text{otherwise}, \end{cases} \tag{6.13}$$

where $\epsilon > 0$. Corresponding to the modification, the chemical potential is changed to

$$\mu^{ideal} = \begin{cases} RT(ln(\epsilon) - 1) + RT(\frac{1}{\epsilon}n_i), & if \quad n_i < \epsilon, \\ RTln(n_i), \text{otherwise}. \end{cases} \tag{6.14}$$

We consider a mixture of methane and n-decane in a square domain with the length of 80 nm on each side. We denote the molar density of n-decane as n_1 and that of methane as n_2, respectively. In Table 6.3, we list the dimensional parameters related to these two components. Other parameter values [11] are chosen as follows

$$\eta_1 = \eta_2 = 1 \times 10^{-4} Pa \cdot s, \quad \bar{\eta}_1 = \bar{\eta}_2 = 0.33 \times 10^{-4} Pa \cdot s, \quad M_1 = 1 \times 10^{-12} m^2 \cdot s^{-1},$$

$$\kappa_{n_1 n_1} = 1.1246 \times 10^{-18}, \quad \kappa_{n_2 n_2} = 2.8649 \times 10^{-20}, \quad \kappa_{n_1 n_2} = 8.9748 \times 10^{-20}. \tag{6.15}$$

The gas constant is $R = 8.3144598 J \cdot mol^{-1} \cdot K^{-1}$, the temperature $T = 330K$. The initial conditions are given by

$$n_i = \begin{cases} n_i^{liquid}, & (x^2 + y^2) \leq (r_1 + r_2 \times cos(n \times arctan(\frac{x}{y})))^2 \quad in \quad [-4 \times 10^{-8} m, 4 \times 10^{-8} m]^2, \\ n_i^{gas}, & otherwise \quad in \quad [-4 \times 10^{-8} m, 4 \times 10^{-8} m]^2, \end{cases} \tag{6.16}$$

Table 6.4: Dimensionless critical parameters

Symbol	T_c	P_c	w	m
n-decane $(C_{10}H_{22})$	2.2626	1.3495	0.4884	8.8688
methane (CH_4)	0.6980	2.9513	0.01142	1

where $r_1 = 1$, $r_2 = 0.2$, $n = 8$ and

$$
\begin{aligned}
n_1^{liquid} &= 3814.6 mol \cdot m^{-3}, \qquad n_1^{gas} = 26.5 mol \cdot m^{-3}, \\
n_2^{liquid} &= 3513.2 mol \cdot m^{-3}, \qquad n_2^{gas} = 7133.9 mol \cdot m^{-3}.
\end{aligned}
\tag{6.17}
$$

If we take characteristic molar density $n_0 = 10^3 mol \cdot m^{-3}$, characteristic density $\rho_0 = n_0 m_2 = 16.0428 kg \cdot m^{-3}$, characteristic length $h = 2 \times 10^{-8} m$, characteristic time $t_0 = 6.4171 \times 10^{-11} s$, and characteristic temperature $T_0 = 273 K$, we obtain dimensionless parameter values as follows

$$
\begin{aligned}
Re_{1s} = Re_{2s} &= 1, \quad Re_{1v} = Re_{2v} = 3, \quad M_1 = 9.7136 \times 10^{-4}, \\
\kappa_{n_1 n_1} &= 0.0018, \quad \kappa_{n_2 n_2} = 4.5961 \times 10^{-5}, \quad \kappa_{n_1 n_2} = 1.4398 \times 10^{-4}.
\end{aligned}
\tag{6.18}
$$

Other dimensionless critical parameters of the methane and n-decane are given in table 6.4. Through the non-dimensionalization, the gas constant R results in a constant $R_0 = 1.4566$, the dimensionless temperature $T = 1.2088$. The corresponding dimensionless initial conditions become

$$
n_i = \begin{cases} n_i^{liquid}, & (x^2 + y^2) \leq (r_1 + r_2 \times cos(n \times arctan(\frac{x}{y})))^2 \quad in \quad [-2, 2] \times [-2, 2], \\ n_i^{gas}, & otherwise \quad in \quad [-2, 2] \times [-2, 2], \end{cases}
\tag{6.19}
$$

where $r_1 = 1$, $r_2 = 0.2$, $n = 8$ and

$$
n_1^{liquid} = 3.8146, \quad n_1^{gas} = 0.0265, \quad n_2^{liquid} = 3.5132, \quad n_2^{gas} = 7.1339.
\tag{6.20}
$$

Shown in Figure 6.5, we perturb the initial condition with certain roughness on the interface, which is unstable due to the surface tension. As time elapses, the roughness vanishes, leading to a surface with the minimal surface tension on it, shown in Figure (6.7-b). The corresponding time evolution of velocities are depicted in Figure 6.6, which show that hydrodynamics indeed speed up the evolution of the system to the steady states.

6.3.1 Density profiles and mass absorption at the interface in equilibrium

Near equilibrium ($t = 6000$), we show the density profiles of the two fluid components at $y = 0$ in Figure (6.8-a) and observe mass absorption of methane at the interface. At the equilibrium of co-existing phases, two (or more) bulk phases have equal chemical potentials, i.e. the corresponding
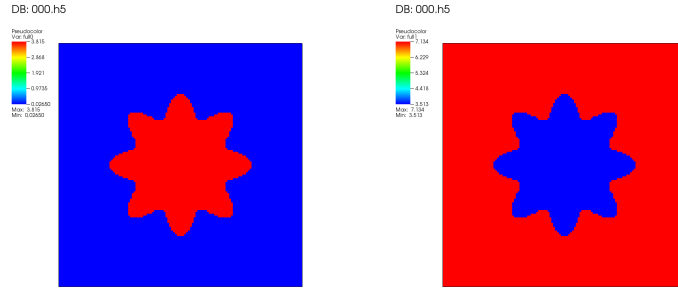
(a) Initial condition of n-decane ($C_{10}H_{22}$)
(b) Initial condition of methane (CH_4)

Figure 6.5: Initial conditions of two components in gas-liquid mixture

bulk free energies lie on the same tangent line (or surface). For the Peng-Robinson free energy, it is not straightforward to find the equilibrium states by observing the graph of the free energy function directly. Following the work reported in [31, 37], we subtract the tangent line (or surface) from the Helmholtz free energy density function to make the equilibrium states as the minimum points, which are then easily observed,

$$h_m(\mathbf{n}, T) = h(\mathbf{n}, T) - \sum_{i=1}^{2} \mu_i^0 n_i, \tag{6.21}$$

where $\mu_i^0, i = 1, 2$ represent the chemical potential of the ith component at the bulk equilibrium state. We show the modified free energy contour in Figure (6.8-b). The circled curve represents the energy path of density profiles at the equilibrium state. To avoid high free energy, n-decane and methane change from one equilibrium state (Gas) to another equilibrium state (Liquid) through the saddle point of the free energy surface. Thus, the methane has a higher density on the interface than in the bulk states, leading to the mass absorption phenomena at the interface.

The total energy and total mass difference with the initial condition for each component are shown in Figure 6.7, which verifies energy stability and mass conservation of our numerical scheme.

This numerical experiment not only demonstrates that our mathematical model can be applied to study thermodynamic and hydrodynamic properties of the fluid mixture in an application relevant to the petroleum industry, but also showcases that our numerical scheme can handle the Navier-Stokes-Cahn-Hilliard equation system with a highly nonlinear free energy (6.12).

7   Conclusion

In this paper, we present a second order, fully-discrete, linear and unconditionally energy stable numerical scheme for the hydrodynamic phase field model of compressible fluid flow. Firstly, we reformulate the model by introducing a couple of intermediate variables, based on the Energy Quadratization approach. Using the reformulated model equations, we develop a second order, energy stable, semi-discrete numerical scheme in time. Then, we obtain a fully discrete numerical
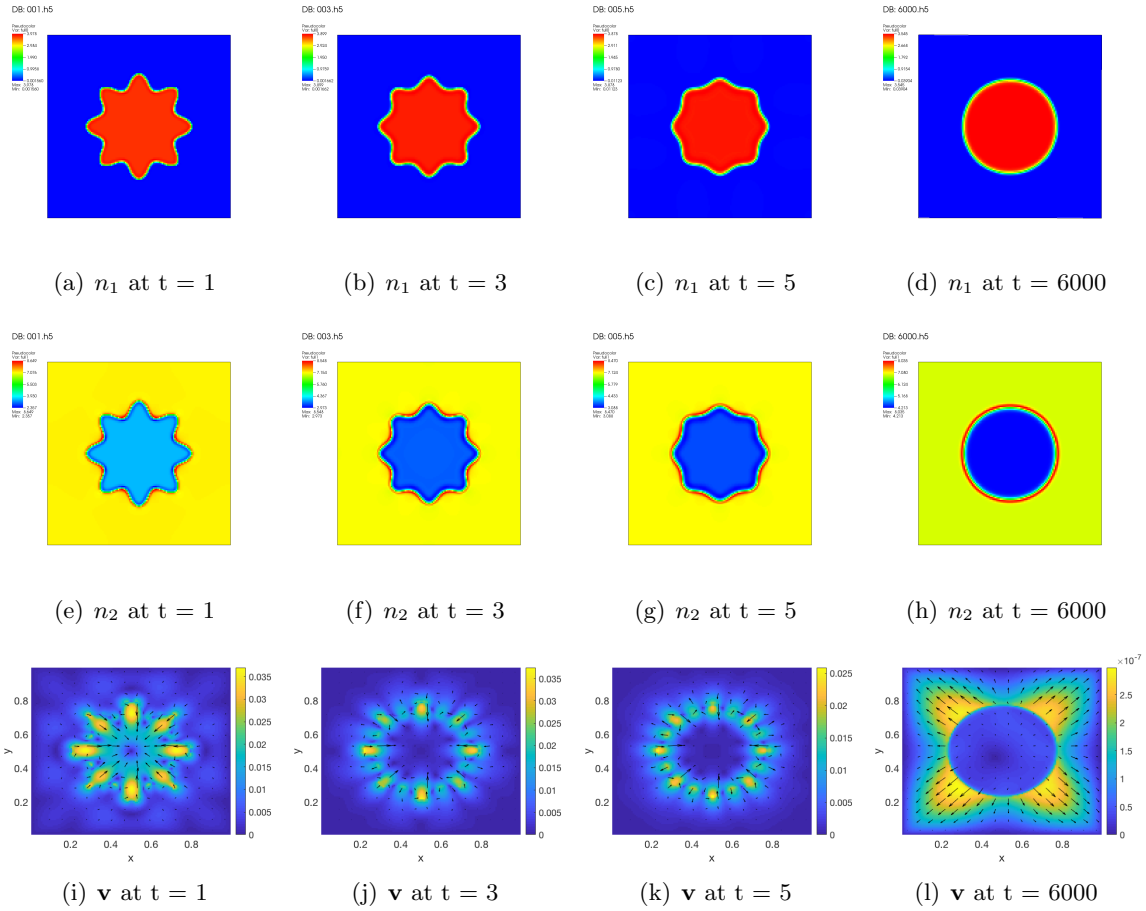
Figure 6.6: (a-d) Snapshots of n_1 at t = 1, 3, 5, 6000. (e-h) Snapshots of n_2. (i-l) The corresponding velocity fields.

(a) Total Energy

(b) Surface tension

(c) The difference of total mass of (d) The difference of total mass of
the component 2 with its initial to- the component 2 with its initial to-
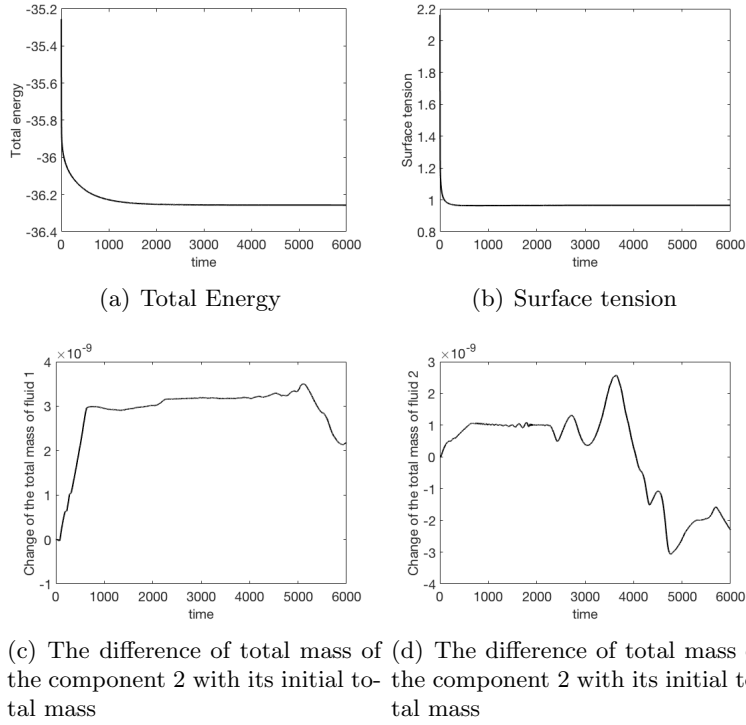tal mass   tal mass

Figure 6.7: (a) Total energy of the system (3.5) with the Peng-Robinson bulk free energy (6.12); (b) Surface tension of the mixture; (c, d) Total mass of the component 1 and 2 on the rectangular domain $\Omega = [-2, 2] \times [-2, 2]$, solved in the system (3.5) with the Peng-Robinson bulk free energy (6.12). (e) Density profiles of n-decane and methane (y = 0) at the equilibrium state; (f) Free energy contour. Green points represent the densities of n-decane and methane at bulk area and red circles represent their densities on the interface at equilibrium state.

(a) Density profiles at the equilib- (b) Free energy contour at the
rium state (t = 6000)   equilibrium state (t = 6000)

Figure 6.8: (a) Density profiles of n-decane and methane (y = 0) at the equilibrium state; (b) Free energy contour. Green points represent the densities of n-decane and methane at bulk area and red circles represent their densities on the interface at equilibrium state.
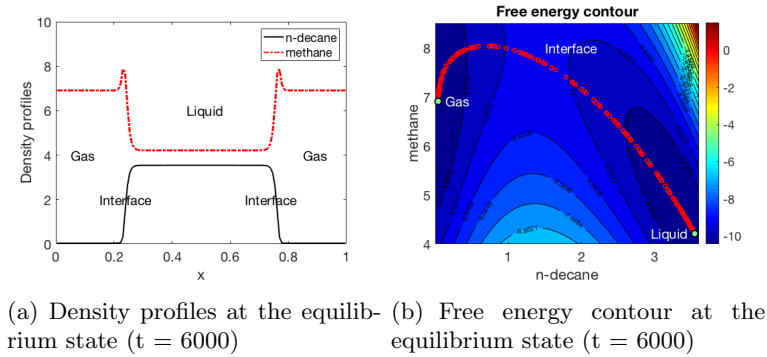
30

scheme applying the finite difference method on the staggered grid, which preserves a fully discrete energy dissipation law. In addition, the well-posedness of the linear system resulting from the linear numerical scheme is proved rigorously. Several numerical experiments are presented to verify the accuracy, stability and efficiency of our numerical scheme. The comparison between the simulations with and without hydrodynamics is used to demonstrate the mixing role played by hydrodynamics in phase separation phenomena in binary compressible fluid flows. The scheme can be readily extended to models N-component compressible fluid flows with $N > 2$.

8 Appendix

8.1 Linear system resulting from the numerical scheme

We summarize the linear system resulting from the numerical scheme as follows.

$$
\begin{cases}
\{2\frac{\rho_1}{\Delta t} + d_x(A_x(\overline{\rho}_1^{n+1/2}\overline{\frac{1}{\sqrt{\rho}}}^{n+1/2})u) + d_y(A_y(\overline{\rho}_1^{n+1/2}\overline{\frac{1}{\sqrt{\rho}}}^{n+1/2})v) = \\
M_1\Delta_h\mu_1 - M_1\Delta_h\mu_2 + g_1\}|_{i,j}, i = 1,\cdots,N_x, j = 1,\cdots,N_y, \\
\\
\{2\frac{\rho_2}{\Delta t} + d_x(A_x(\overline{\rho}_2^{n+1/2}\overline{\frac{1}{\sqrt{\rho}}}^{n+1/2})u) + d_y(A_y(\overline{\rho}_2^{n+1/2}\overline{\frac{1}{\sqrt{\rho}}}^{n+1/2})v) = \\
-M_1\Delta_h\mu_1 + M_1\Delta_h\mu_2 + g_2\}|_{i,j}, i = 1,\cdots,N_x, j = 1,\cdots,N_y, \\
\\
\{2\frac{u}{\Delta t} + \frac{1}{2}(\overline{u}^{n+1/2}D_x(\overline{\frac{1}{\sqrt{\rho}}}^{n+1/2}a_x u) + A_x(\overline{\frac{1}{\sqrt{\rho}}}^{n+1/2}d_x(\overline{u}^{n+1/2}u))) \\
+\frac{1}{2}(a_x(A_x\overline{v}^{n+1/2}D_y(A_x(\overline{\frac{1}{\sqrt{\rho}}}^{n+1/2})u)) + A_x(\overline{\frac{1}{\sqrt{\rho}}}^{n+1/2})d_y(A_yuA_x(\overline{v}^{n+1/2})) \\
= A_x(\overline{\frac{1}{\sqrt{\rho}}}^{n+1/2})(D_x(\frac{1}{Re_s}d_x(A_x(\overline{\frac{1}{\sqrt{\rho}}}^{n+1/2})u)) + d_y(A_x(A_y\frac{1}{Re_s})D_y(A_x(\overline{\frac{1}{\sqrt{\rho}}}^{n+1/2})u))) \\
+A_x(\overline{\frac{1}{\sqrt{\rho}}}^{n+1/2})D_x(\frac{1}{Re_s}d_x(A_x(\overline{\frac{1}{\sqrt{\rho}}}^{n+1/2})u)) + A_x(\overline{\frac{1}{\sqrt{\rho}}}^{n+1/2})d_y(A_x(A_y\frac{1}{Re_s})D_x(A_y(\overline{\frac{1}{\sqrt{\rho}}}^{n+1/2})v)) \\
+A_x(\overline{\frac{1}{\sqrt{\rho}}}^{n+1/2})D_x(\frac{1}{Re_v}d_x(A_x(\overline{\frac{1}{\sqrt{\rho}}}^{n+1/2})u)) + A_x(\overline{\frac{1}{\sqrt{\rho}}}^{n+1/2})D_x(\frac{1}{Re_v}d_y(A_y(\overline{\frac{1}{\sqrt{\rho}}}^{n+1/2})v)) \\
-A_x(\overline{\rho_1}^{n+1/2}\overline{\frac{1}{\sqrt{\rho}}}^{n+1/2})D_x(\mu_1) - A_x(\overline{\rho_2}^{n+1/2}\overline{\frac{1}{\sqrt{\rho}}}^{n+1/2})D_x(\mu_2) + g_3\}|_{i+\frac{1}{2},j}, \\
i = 1,\cdots,N_x-1, j = 1,\cdots,N_y, \\
\\
\{2\frac{v}{\Delta t} + \frac{1}{2}(a_x(A_y\overline{u}^{n+1/2}D_x(A_y(\overline{\frac{1}{\sqrt{\rho}}}^{n+1/2})v)) + A_y(\overline{\frac{1}{\sqrt{\rho}}}^{n+1/2})d_x(A_y\overline{u}^{n+1/2}A_xv^{n+1/2})) \\
+\frac{1}{2}(\overline{v}^{n+1/2}D_y(\overline{\frac{1}{\sqrt{\rho}}}^{n+1/2}a_yv^{n+1/2}) + A_y(\overline{\frac{1}{\sqrt{\rho}}}^{n+1/2}d_y(\overline{v}^{n+1/2}v^{n+1/2}))) \\
= A_y(\overline{\frac{1}{\sqrt{\rho}}}^{n+1/2})(d_x(A_x(A_y\frac{1}{Re_s})D_x(A_y(\overline{\frac{1}{\sqrt{\rho}}}^{n+1/2})v)) + D_y(\frac{1}{Re_s}d_y(A_y(\overline{\frac{1}{\sqrt{\rho}}}^{n+1/2})v))) \\
+A_y(\overline{\frac{1}{\sqrt{\rho}}}^{n+1/2})d_x(A_x(A_y\frac{1}{Re_s})D_y(A_x(\overline{\frac{1}{\sqrt{\rho}}}^{n+1/2})u)) + A_y(\overline{\frac{1}{\sqrt{\rho}}}^{n+1/2})D_y(\frac{1}{Re_s}d_y(A_y(\overline{\frac{1}{\sqrt{\rho}}}^{n+1/2})v)) \\
+A_y(\overline{\frac{1}{\sqrt{\rho}}}^{n+1/2})D_y(\frac{1}{Re_v}d_x(A_x(\overline{\frac{1}{\sqrt{\rho}}}^{n+1/2})u)) + A_y(\overline{\frac{1}{\sqrt{\rho}}}^{n+1/2})D_y(\frac{1}{Re_v}d_y(A_y(\overline{\frac{1}{\sqrt{\rho}}}^{n+1/2})v)) \\
-A_y(\overline{\rho_1}^{n+1/2}\overline{\frac{1}{\sqrt{\rho}}}^{n+1/2})D_y(\mu_1) - A_y(\overline{\rho_2}^{n+1/2}\overline{\frac{1}{\sqrt{\rho}}}^{n+1/2})D_y(\mu_2) + g_4\}|_{i,j+\frac{1}{2}}, \\
i = 1,\cdots,N_x, j = 1,\cdots,N_y-1.
\end{cases} \tag{8.1}
$$

$$\begin{cases} \{4\frac{q_1}{\Delta t} = 4\overline{\frac{\partial q_1}{\partial \rho_1}}^{n+1/2}\frac{\rho_1}{\Delta t} + 4\overline{\frac{\partial q_1}{\partial \rho_2}}^{n+1/2}\frac{\rho_2}{\Delta t} + g_5\}|_{i,j}, i = 1, \cdots, N_x, j = 1, \cdots, N_y, \\[3mm] \{-\frac{2}{\Delta t}\mu_1 = -4q_1\frac{1}{\Delta t}\overline{\frac{\partial q_1}{\partial \rho_1}}^{n+1/2} + \frac{2}{\Delta t}\kappa_{\rho_1\rho_1}\Delta_h\rho_1 + \frac{2}{\Delta t}\kappa_{\rho_1\rho_2}\Delta_h\rho_2 + g_6, \}|_{i,j}, \\ i = 1, \cdots, N_x, j = 1, \cdots, N_y, \\[3mm] \{-\frac{2}{\Delta t}\mu_2 = -4q_1\frac{1}{\Delta t}\overline{\frac{\partial q_1}{\partial \rho_2}}^{n+1/2} + \frac{2}{\Delta t}\kappa_{\rho_2\rho_2}\Delta_h\rho_2 + \frac{2}{\Delta t}\kappa_{\rho_1\rho_2}\Delta_h\rho_1 + g_7, \}|_{i,j}, \\ i = 1, \cdots, N_x, j = 1, \cdots, N_y, \end{cases} \tag{8.2}$$

where $\rho_i, \mu_i, i = 1, 2$ and q_1 satisfy discrete homogeneous Neumann boundary conditions (5.8), u, v the discrete homogeneous Dirichlet boundary conditions (5.9). We define $\mathbf{D}_h$ as

$$\begin{pmatrix} d_x(A_x(\overline{\frac{1}{\sqrt{\rho}}}^{n+1/2})u)) & \frac{1}{2}(D_x(A_y(\overline{\frac{1}{\sqrt{\rho}}}^{n+1/2})v) + D_y(A_x(\overline{\frac{1}{\sqrt{\rho}}}^{n+1/2})u))) \\ \frac{1}{2}(D_x(A_y(\overline{\frac{1}{\sqrt{\rho}}}^{n+1/2})v) + D_y(A_x(\overline{\frac{1}{\sqrt{\rho}}}^{n+1/2})u))) & d_y(A_y(\overline{\frac{1}{\sqrt{\rho}}}^{n+1/2})v)) \end{pmatrix} \tag{8.3}$$

References

[1] Helmut Abels. On a diffuse interface model for two-phase flows of viscous, incompressible fluids with matched densities. *Archive for Rational Mechanics and Analysis*, 194(2):463–506, Nov 2009.

[2] S. Aland, S. Egerer, J. Lowengrub, and A. Voigt. Diffuse interface models of locally inextensible vesicles in a viscous fluid. *Journal of Computational Physics*, 277:32–47, 2014.

[3] S. Aland, J. Lowengrub, and A. Voigt. Particles at fluid-fluid interfaces: a new Navier-Stokes-Cahn-Hilliard surface-phase-field model. *Physical Review E*, 86(4), 2012.

[4] A. Bertozzi, S. Esedoglu, and A. Gillette. Inpainting of binary images using the cahn-hilliard equation. *IEEE Trans Image Process.*, 16(1):285–291, 2007.

[5] M. Borden, C. Verhoosej, M. Scott, T. Hughes, and C. Landis. A phase-field description of dynamic brittle fracture. *Computer Methods in Applied Mechanics and Engineering*, 217(220):77–95, 2012.

[6] B. Camley, Y. Zhao, Bo Li, H. Levine, and W. Rappel. Crawling and turning in a minimal reaction-diffusion cell motility model: coupling cell shape and biochemistry. *Physical Review E*, 95(012401), 2017.

[7] L. Q. Chen and W. Yang. Computer simulation of the dynamics of a quenched system with large number of non-conserved order parameters. *Phys. Rev. B*, 60:15752–15756, 1994.

[8] Wenbin Chen, Wenqiang Feng, Yuan Liu, Cheng Wang, and Steven M. Wise. A second order energy stable scheme for the cahn-hilliard-hele-shaw equations. *Discrete & Continuous Dynamical Systems - B*, 22:1, 2018.

[9] Y. Chen and J. Shen. Efficient adaptive energy stable schemes for the incompressible cahn-hilliard navier-stokes phase-field models. *Journal of Computational Physics*, 308:40–56, 2016.

[10] Kelong Cheng, Wenqiang Feng, Cheng Wang, and Steven M. Wise. An energy stable fourth order finite difference scheme for the cahn-hilliard equation. *Journal of Computational and Applied Mathematics*, 2018.

[11] Alvin S. Cullick and Melwyn L. Mathis. Densities and viscosities of mixtures of carbon dioxide and n-decane from 310 to 403 k and 7 to 30 mpa. *Journal of Chemical & Engineering Data*, 29(4):393–396, 1984.

[12] M. Doi and S. F. Edwards. *The Theory of Polymer Dynamics*. Oxford Science Publication, 1986.

[13] Q. Du, C. Liu, R. Ryham, and X. Wang. A phase field formulation of the willmore problem. *Nonlinearity*, 18:1249–1267, 2005.

[14] C. M. Elliott and A. M. Stuart. The global dynamics of discrete semilinear parabolic equations. *SIAM Journal of Numerical Analysis*, 30:1622–1663, 1993.

[15] D. Eyre. Unconditionally gradient stable time marching the Cahn-Hilliard equation. *Computational and mathematical models of microstructural evolution (San Francisco, CA, 1998)*, 529:39–46, 1998.

[16] Nir Gavish, Gurgen Hayrapetyan, Keith Promislow, and Li Yang. Curvature driven flow of bilayer interfaces. *Physica D.: Nonlinear Phenomena*, 240:675–693, 2011.

[17] Yuezheng Gong, Jia Zhao, and Qi Wang. An energy stable algorithm for a quasi-incompressible hydrodynamic phase-field model of viscous fluid mixtures with variable densities and viscosities. *Computer Physics Communications*, 219:20 – 34, 2017.

[18] Yuezheng Gong, Jia Zhao, and Qi Wang. Second order fully discrete energy stable methods on staggered grids for hydrodynamic phase field models of binary viscous fluids. *SIAM Journal on Scientific Computing*, 40(2):B528–B553, 2018.

[19] Yuezheng Gong, Jia Zhao, Xiaogang Yang, and Qi Wang. Fully discrete second-order linear schemes for hydrodynamic phase field models of binary viscous fluid flows with variable densities. *SIAM Journal on Scientific Computing*, 40(1):B138–B167, 2018.

[20] Edouard Hannezo, Alice Coucke, and Jean-François Joanny. Interplay of migratory and division forces as a generic mechanism for stem cell patterns. *Phys. Rev. E*, 93:022405, Feb 2016.

[21] P. C. Hohenberg and B. I. Halperin. Theory of dynamic critical phenomena. *Reviews of Modern Physics*, 49(3):435–479, 1977.

[22] Maryna Kapustina, Denis Tsygankov, Jia Zhao, Timothy Wessler, Xiaofeng Yang, Alex Chen, Nathan Roach, Timothy C. Elston, Qi Wang, Ken Jacobson, and M. Gregory Forest. Modeling the excess cell surface stored in a complex morphology of bleb-like protrusions. *PLOS Computational Biology*, 12(3):1–25, 03 2016.

[23] Jisheng Kou and Shuyu Sun. Thermodynamically consistent modeling and simulation of multi-component two-phase flow model with partial miscibility. *Computer Methods in Applied Mechanics and Engineering*, 331:623 – 649, 2018.

[24] Jisheng Kou, Shuyu Sun, and Xiuhua Wang. Linearly decoupled energy-stable numerical methods for multi-component two-phase compressible flow. *arXiv preprint arXiv:1712.02222*, 2017.

[25] Y. Li and J. Kim. Multiphase image segmentation using a phase-field model. *Computers and Mathematics with Applications*, 62:737–745, 2011.

[26] Hong Lin and Yuan-Yuan Duan. Surface tension measurements of propane (r-290) and isobutane (r-600a) from (253 to 333) k. *Journal of Chemical & Engineering Data*, 48(5):1360–1363, 2003.

[27] C. Liu and J. Shen. A phase field model for the mixture of two incompressible fluids and its approximation by a Fourier-spectral method. *Physica D*, 179(3):211–228, 2003.

[28] J. Lober, F. Ziebert, and I. S. Aranson. Modeling crawling cell movement on soft engineered substrates. *Soft Matter*, 10:1365, 2014.

[29] J. Lowengrub, A. Ratz, and A. Voigt. Phase field modeling of the dynamics of multicomponent vesicles spinodal decomposition coarsening budding and fission. *Physical Review E*, 79(3), 2009.

[30] J. S. Lowengrub and L. Truskinovsky. Quasi incompressible Cahn-Hilliard fluids and topological transitions. *Proceedings of the Royal Society A*, 454:2617–2654, 1998.

[31] Xiaoqun Mu, Florian Frank, Faruk O. Alpak, and Walter G. Chapman. Stabilized density gradient theory algorithm for modeling interfacial properties of pure and mixed systems. *Fluid Phase Equilibria*, 435:118 – 130, 2017.

[32] S. Najem and M. Grant. Coupling actin dynamics to phase-field in modeling neural growth. *Soft Matter*, 11:4476, 2015.

[33] S. Najem and M. Grant. Phase-field model for collective cell migration. *Physical Review E*, 93(052405), 2016.

[34] M. Nonomura. Study on multicellular systems using a phase field model. *PLoS One*, 7(4):0033501, 2012.

[35] Hossein Nourozieh, Bita Bayestehparvin, Mohammad Kariznovi, and Jalal Abedi. Equilibrium properties of (carbon dioxide + n-decane + n-octadecane) systems: Experiments and thermodynamic modeling. *Journal of Chemical & Engineering Data*, 58(5):1236–1243, 2013.

[36] Ding-Yu Peng and Donald B. Robinson. A new two-constant equation of state. *Ind. Eng. Chem. Fundamen.*, 15(1):59–64, 1976.

[37] J. S. Rowlinson and B. Widom. *Molecular Theory of Capillarity*. Clarendon Press, Oxford, 1989.

[38] D. Shao, H. Levine, and W. Pappel. Coupling actin flow, adhesion, and morphology in a computational cell motility model. *PNAS*, 109(18):6855, May 2012.

[39] D. Shao, W. Pappel, and H. Levine. Computational model for cell morphodynamics. *Physical Review Letters*, 105, September 2010.

[40] J. Shen, C. Wang, X. Wang, and S. M. Wise. Second-order convex splitting schemes for gradient flows with ehrlichâschwoebel type energy: Application to thin film epitaxy. *SIAM Journal on Numerical Analysis*, 50(1):105–125, 2012.

[41] J. Shen and X. Yang. Numerical approximations of Allen-Cahn and Cahn-Hilliard equations. *Disc. Conti. Dyn. Sys.-A*, 28:1669–1691, 2010.

[42] Jie Shen, Jie Xu, and Jiang Yang. The scalar auxiliary variable (sav) approach for gradient flows. *Journal of Computational Physics*, 353:407 – 416, 2018.

[43] S. Torabi, J. Lowengrub, A. Voigt, and S. Wise. A new phase-field model for strongly anisotropic systems. *Proceedings of the Royal Society A*, 265:1337–1359, 2009.

[44] X. Wang and Q. Du. Modeling and simulations of multi-component lipid membranes and open membranes via diffuse interface approaches. *Journal of Mathematical Biology*, 56:347–371, 2008.

[45] S. Wise, J. Kim, and J. Lowengrub. Solving the regularized strongly anisotropic cahn-hilliard equation by an adaptive nonlinear multigrid method. *Journal of Computational Physics*, 226(1):414–446, 2007.

[46] S. Wise, J. Lowengrub, H. Frieboes, and B. Cristini. Three dimensional multispecies nonlinear tumor growth i: model and numerical method. *Journal of Theoretical Biology*, 253(3):524–543, 2008.

[47] T. Witkowski, R. Backofen, and A. Voigt. The influence of membrane bound proteins on phase separation and coarsening in cell membranes. *Physical Chemistry Chemical Physics*, 14(42):14403–14712, 2012.

[48] X. Yang. Linear, first and second order and unconditionally energy stable numerical schemes for the phase field model of homopolymer blends. *J. Comput. Phys.*, 327:294–316, 2016.

[49] X. Yang, J. Li, G. Forest, and Q. Wang. Hydrodynamic theories for flows of active liquid crystals and the generalized onsager principle. *Entropy*, 18(6):202, 2016.

[50] J. Zhao, P. Seeluangsawat, and Q. Wang. Modeling antimicrobial tolerance and treatment of heterogeneous biofilms. *Mathematical Biosciences*, 282:1–15, 2016.

[51] J. Zhao, Y. Shen, M. Happasalo, Z. J. Wang, and Q. Wang. A 3d numerical study of antimicrobial persistence in heterogeneous multi-species biofilms. *Journal of Theoretical Biology*, 392:83–98, 2016.

[52] J. Zhao and Q. Wang. Three-dimensional numerical simulations of biofilm dynamics with quorum sensing in a flow cell. *Bulletin of Mathematical Biology*, 79(4):884–919, 2017.

[53] J. Zhao, X. Yang, Y. Gong, and Q. Wang. A novel linear second order unconditionally energy-stable scheme for a hydrodynamic q tensor model for liquid crystals. *Computer Methods in Applied Mechanics and Engineering*, In Press, 2017.

[54] J. Zhao, X. Yang, Y. Gong, and Q. Wang. A novel linear second order unconditionally energy stable scheme for a hydrodynamic q-tensor model of liquid crystals. *in press, DOI: 10.1016/j.cma.2017.01.031, Comput. Meth. Appl. Mech. Engrg.*, 2017.

[55] Jia Zhao and Qi Wang. Modeling cytokinesis of eukaryotic cells driven by the actomyosin contractile ring. *International Journal for Numerical Methods in Biomedical Engineering*, 32(12), 2016.

[56] Jia Zhao, Xiaofeng Yang, Yuezheng Gong, Xueping Zhao, Xiaogang Yang, Jun Li, and Qi Wang. A general strategy for numerical approximations of non-equilibrium models-part i: Thermodynamical systems. *International Journal of Numerical Analysis & Modeling*, 15(6):884–918, 2018.

[57] Jia Zhao, Xiaofeng Yang, Jun Li, and Qi Wang. Energy stable numerical schemes for a hydrodynamic model of nematic liquid crystals. *SIAM. J. Sci. Comput.*, 38:A3264–A3290, 2016.

[58] Xueping Zhao, Tiezheng Qian, and Qi Wang. Thermodynamically consistent phase field models of multi-component compressible fluid flows. *Continuum Mechanics and Thermodynamics, in revision*, 2018.

[59] L. Zhornitskaya and A. Bertozzi. Positivity-preserving numerical schemes for lubrication-type equations. *SIAM Journal of Numerical Analysis*, 37(2):523–555, 2000.

[60] Jingzhi Zhu, Longqing Chen, Jie Shen, and Veena Tikare. Coarsening kinetics from a variable-mobility cahn-hilliard equation: application of a semi-impliciit fourier spectral method. *Physical Review E*, 60:3564, 1999.

[61] F. Ziebert and I. S. Aranson. Effects of adhesion dynamics and substrate compliance on the shape and motility of crawling cells. *PLOS One*, 8(5):e64511, 2013.

[62] F. Ziebert, S. Swaminathan, and I. S. Aranson. Model for self-polarization and motility of keratocyte fragments. *Journal of The Royal Society Interface*, 9:1084–1092, 2012.

[63] D. Zwicker, R. Seyboldt, C. Weber, A. Hyman, and F. Julicher. Growth and division of active droplets provides a model for protocells. *Nature Physics*, 13:408–413, 2017.